



Long-term Creep-Fatigue Interactions in Ni-base Superalloys

Award DE-FE0011722
August 2013 – August 2016
Program Manager: Briggs White

PI: Richard W. Neu

GRAs: Ernesto A. Estrada Rodas, Sanam Gorgan Nejad and Anirudh Bhat

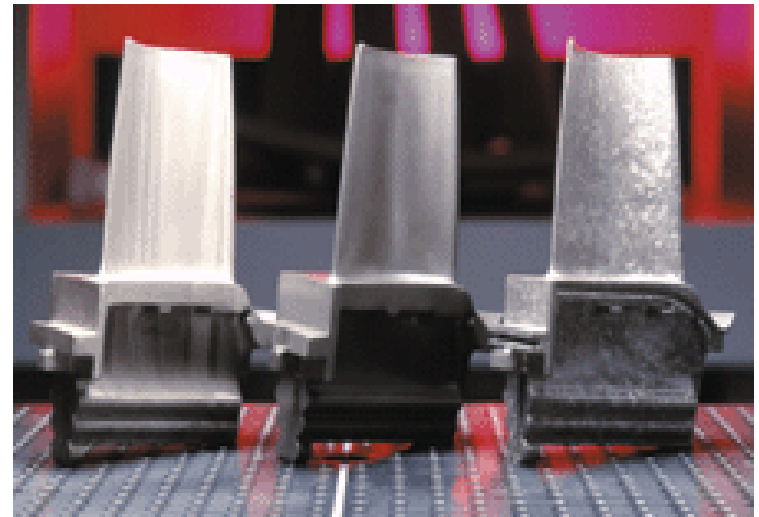
The George W. Woodruff School of Mechanical Engineering
School of Materials Science & Engineering
Georgia Institute of Technology
Atlanta, GA 30332-0405
rick.neu@gatech.edu

University Turbine Systems Research Workshop
Georgia Institute of Technology
November 3-5, 2015



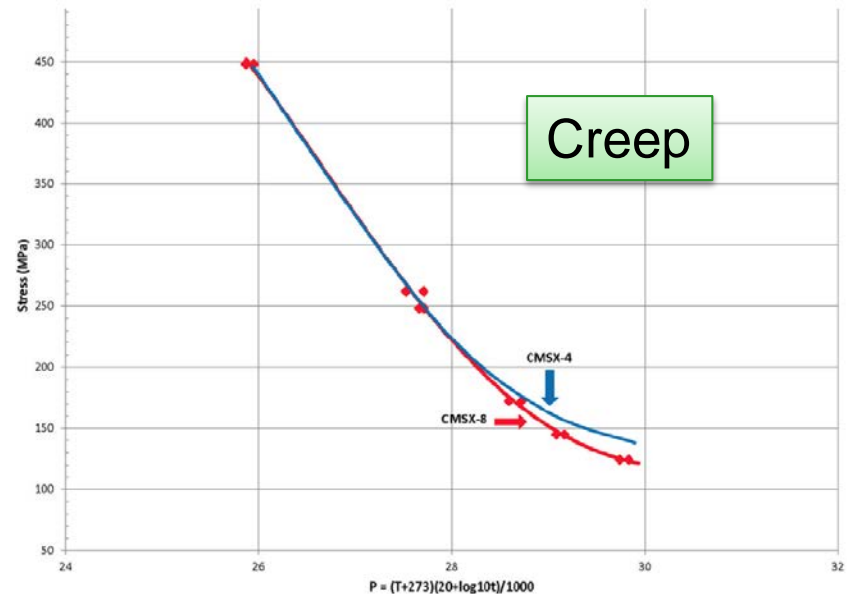
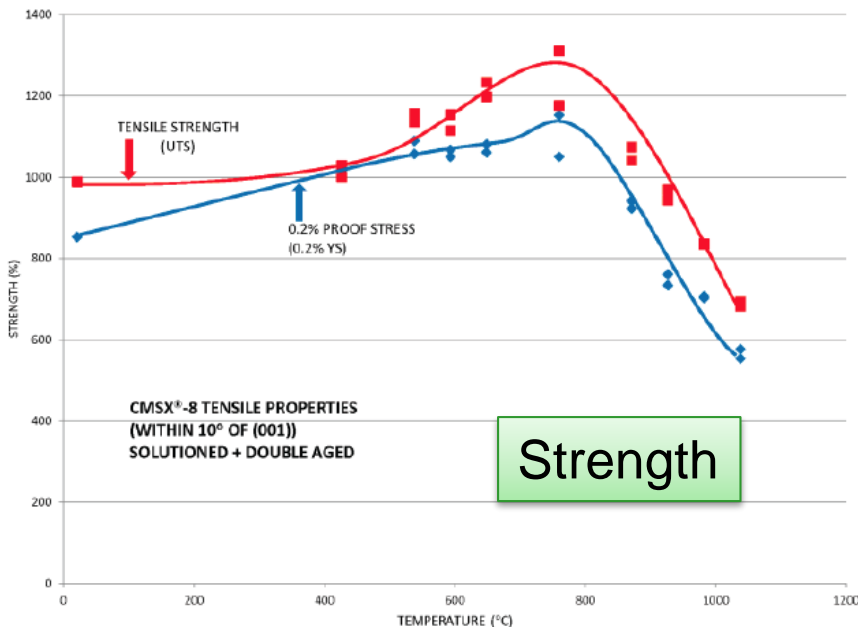
Land-based gas turbines

- drive to increase service temperature to improve efficiency; increase life
- replace large directionally-solidified Ni-base superalloys with single crystal superalloys

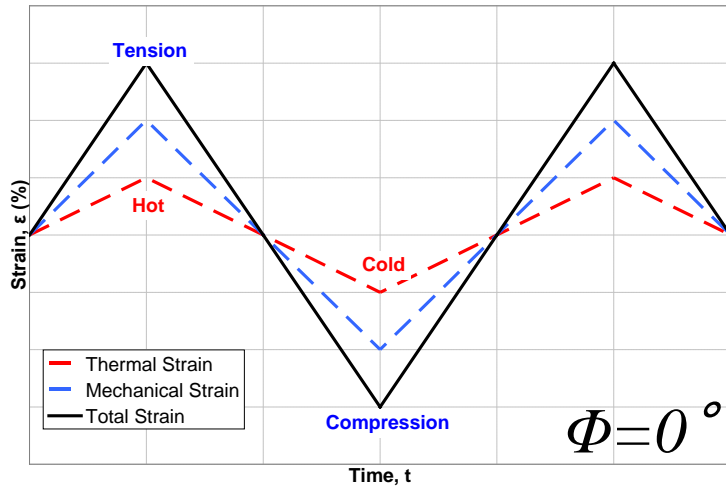


CMSX-8: 1.5% Re "alternative 2nd gen alloy" replacing 3.0% Re containing alloys (e.g., CMSX-4, PWA1484)

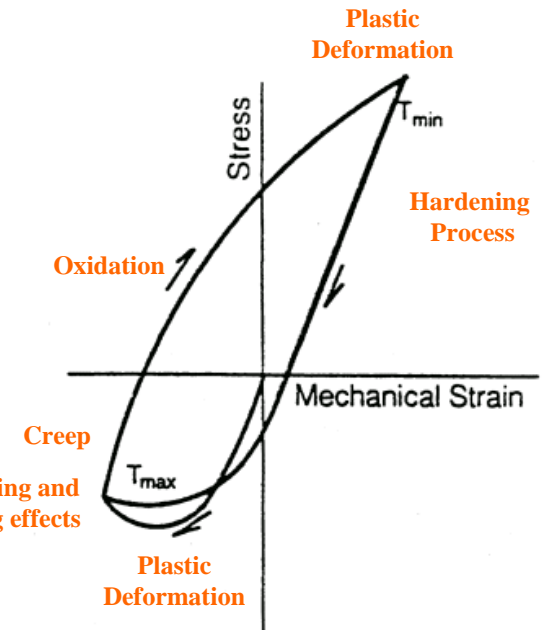
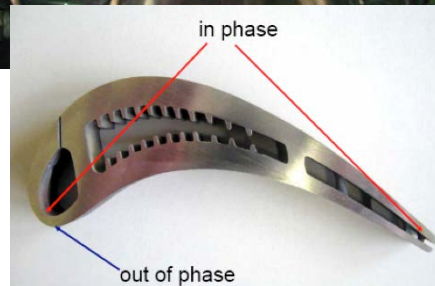
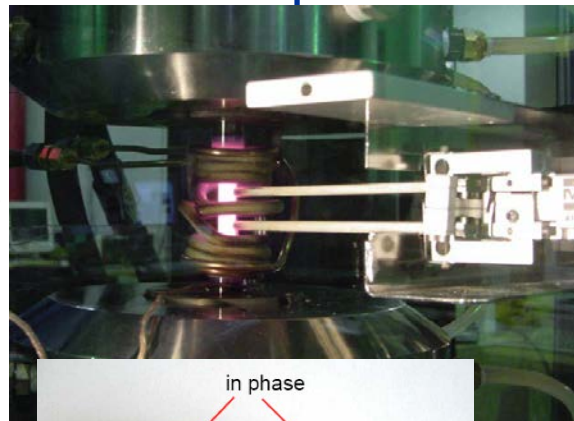
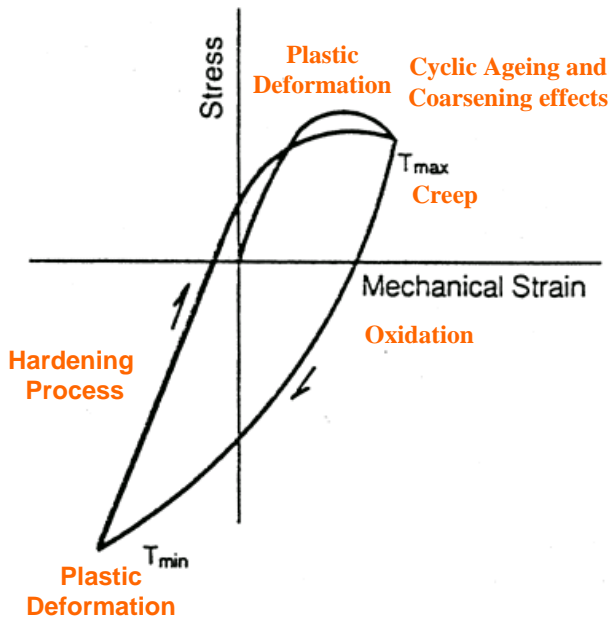
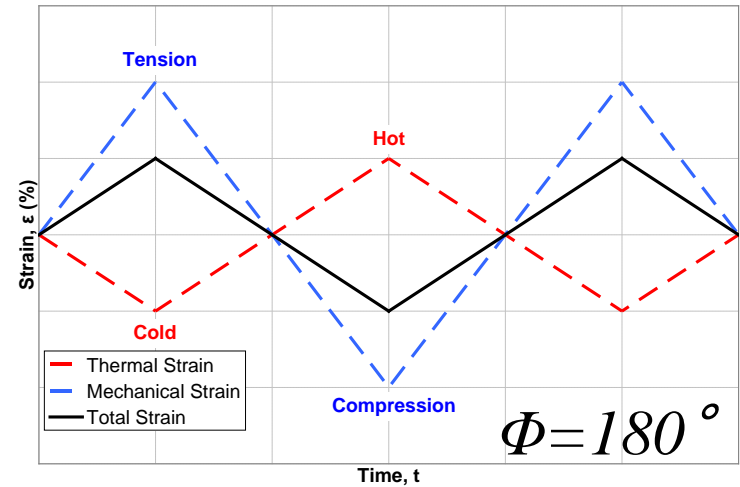
Alloy	Cr	Co	Mo	W	Al	Ti	Ta	Re	Hf	C	B	Zr	Ni
Mar-M247LC-DS	8.4	10.0	0.7	10.0	5.5	1.0	3.0	-	1.5	0.07	0.015	0.05	Bal
CM247LC-DS	8.1	9.2	0.5	9.5	5.6	0.7	3.2	-	1.4	0.07	0.015	0.01	Bal
CMSX-4	6.5	9.0	0.6	6.0	5.6	1.0	6.5	3.0	0.1	-	-	-	Bal
SC16	16	0.17	3.0	0.16	3.5	3.5	3.5	-	-	-	-	-	Bal
PWA1484	5.0	10.0	2.0	6.0	5.6	-	9.0	3.0	0.1	-	-	-	Bal
CMSX-8	5.4	10.0	0.6	8.0	5.7	0.7	8.0	1.5	0.2	-	-	-	Bal



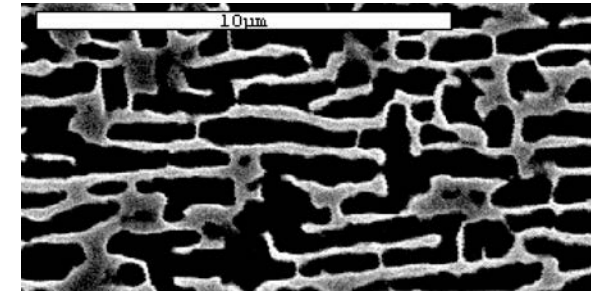
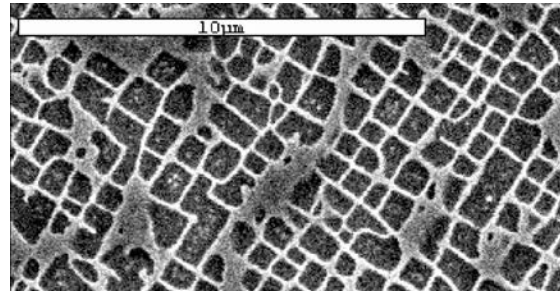
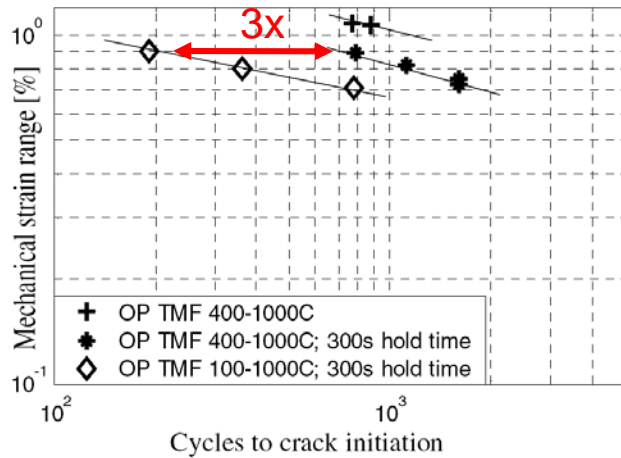
Linear In-Phase (IP)



Linear Out-of-Phase (OP)

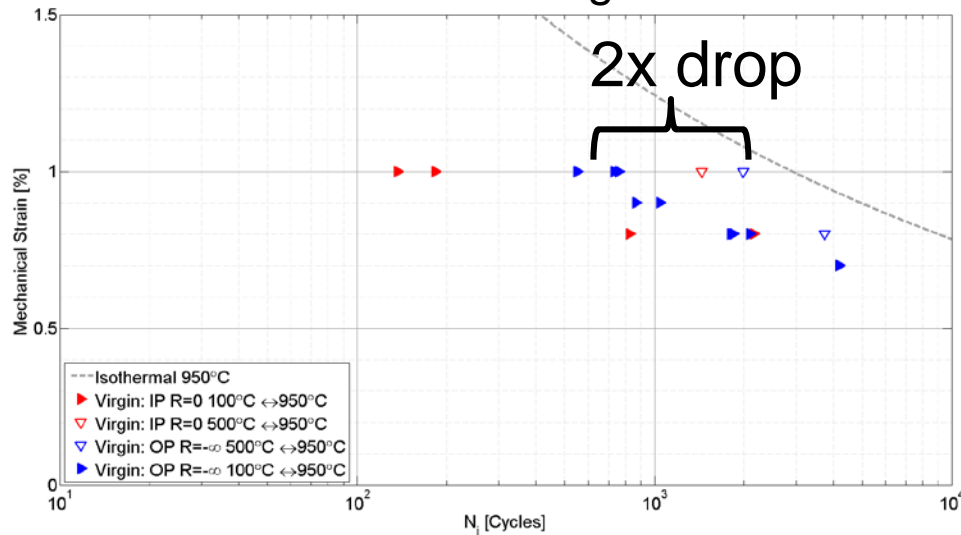


CMSX-4 [001]

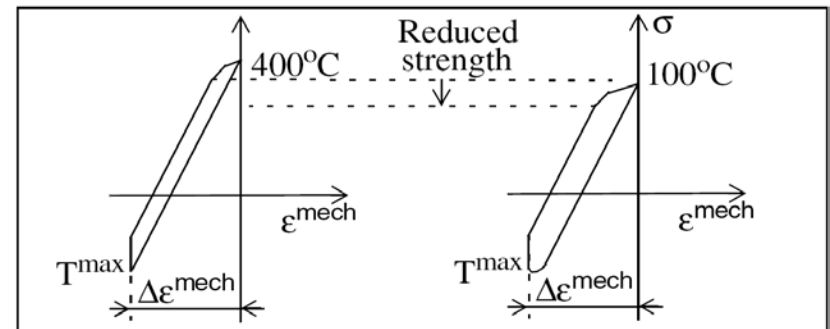


[Arrell et al., 2004]

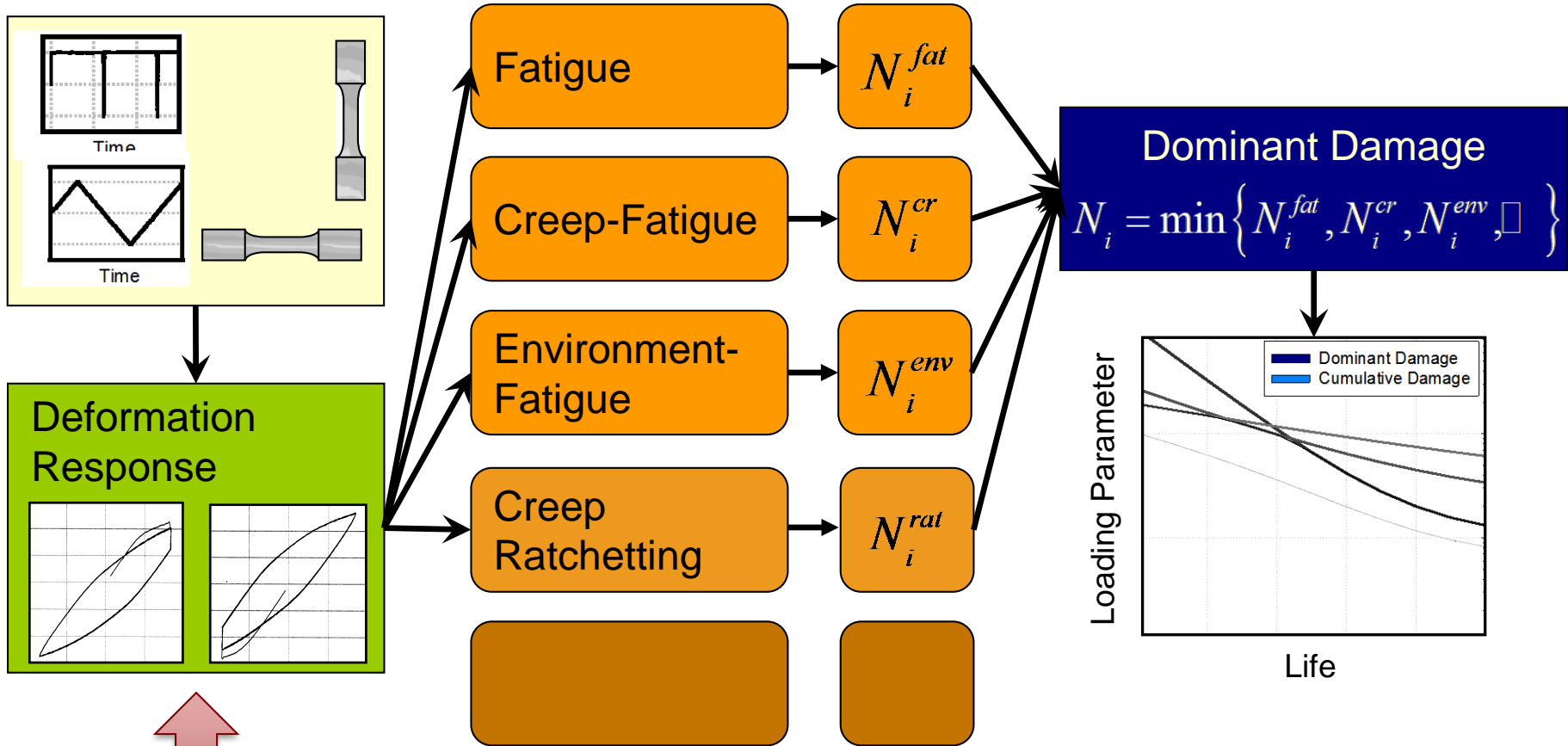
CM247LC DS in Longitudinal Dir.



[Kirka, 2014]



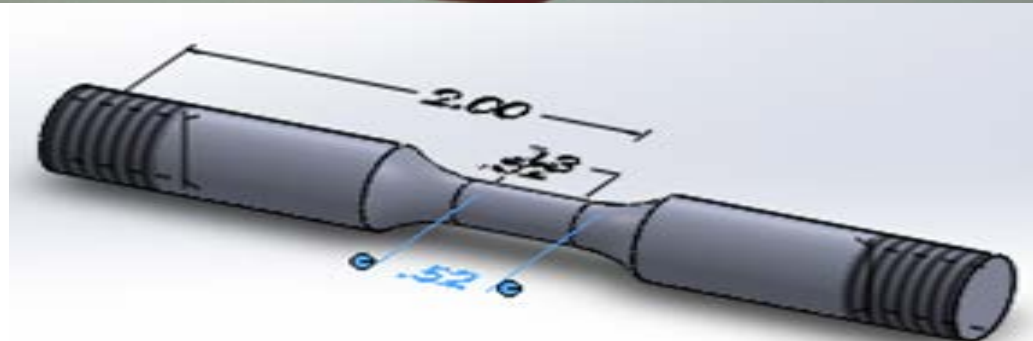
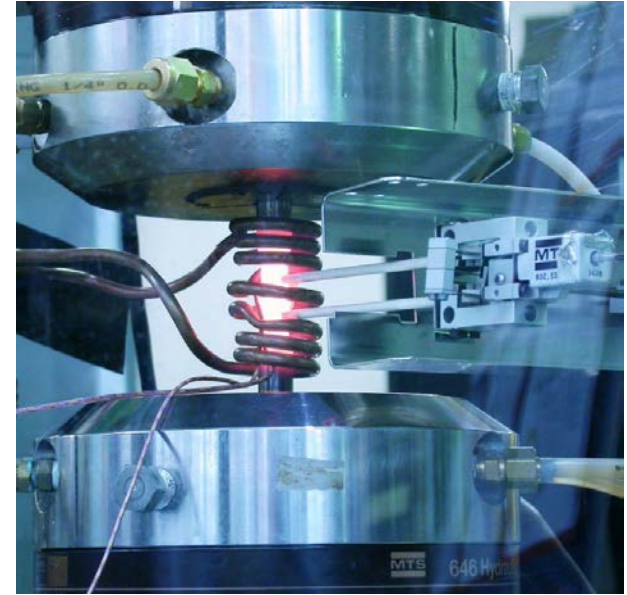
Damage Mechanism Modules



Accurate representations of the deformation response highly critical for predicting crack formation

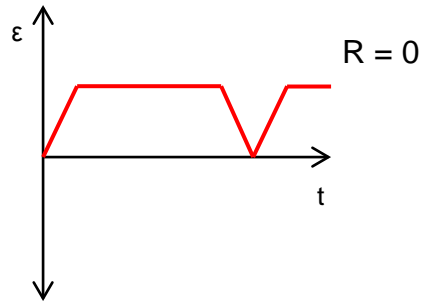
- Creep-fatigue interaction experiments on CMSX-8
- Influence of aging on microstructure and creep-fatigue interactions
- Microstructure-sensitive, temperature-dependent crystal viscoplasticity to capture the creep and cyclic deformation response

- Conventional creep-fatigue (baseline)
 - ASTM E2714-09
- Long-term creep followed by fatigue
- Fatigue followed by long-term creep
- Impact of pre-aging
- Creep-fatigue interaction life analysis
- Orientations: $\langle 001 \rangle$, $\langle 111 \rangle$, $\langle 011 \rangle$
- Application to TMF with long dwells

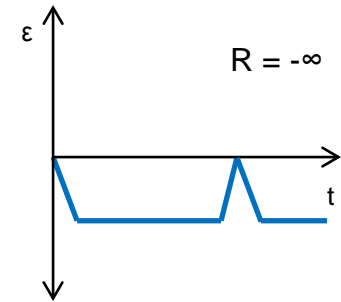
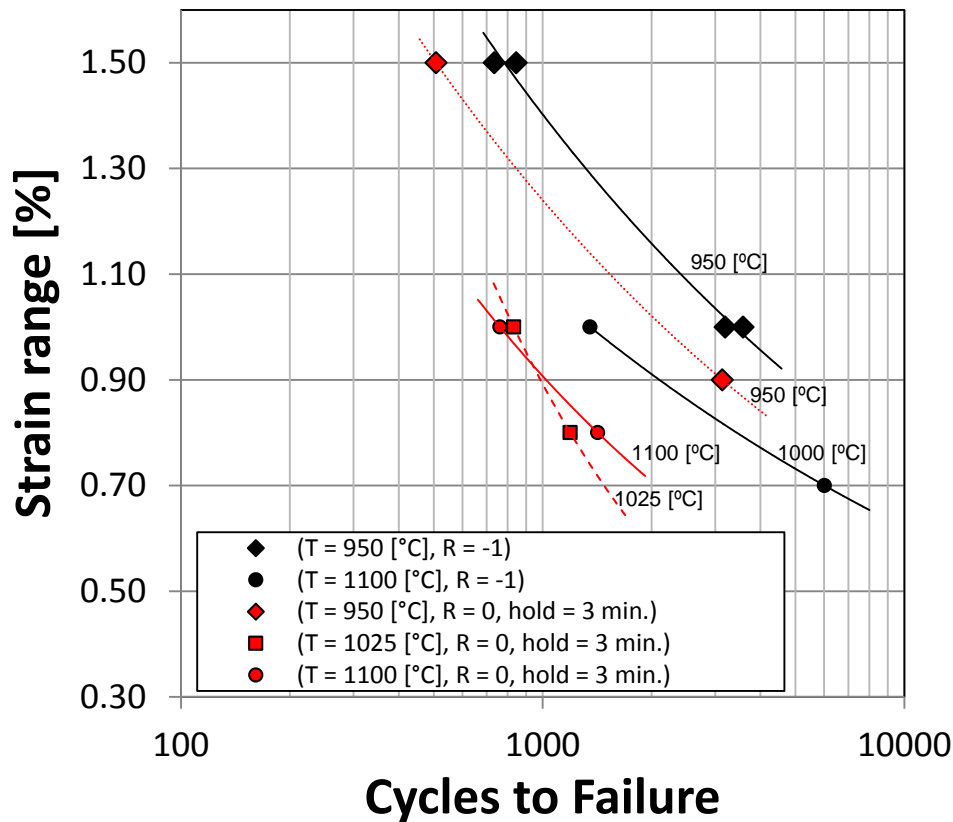


In a creep-fatigue interaction test, life can be controlled by:

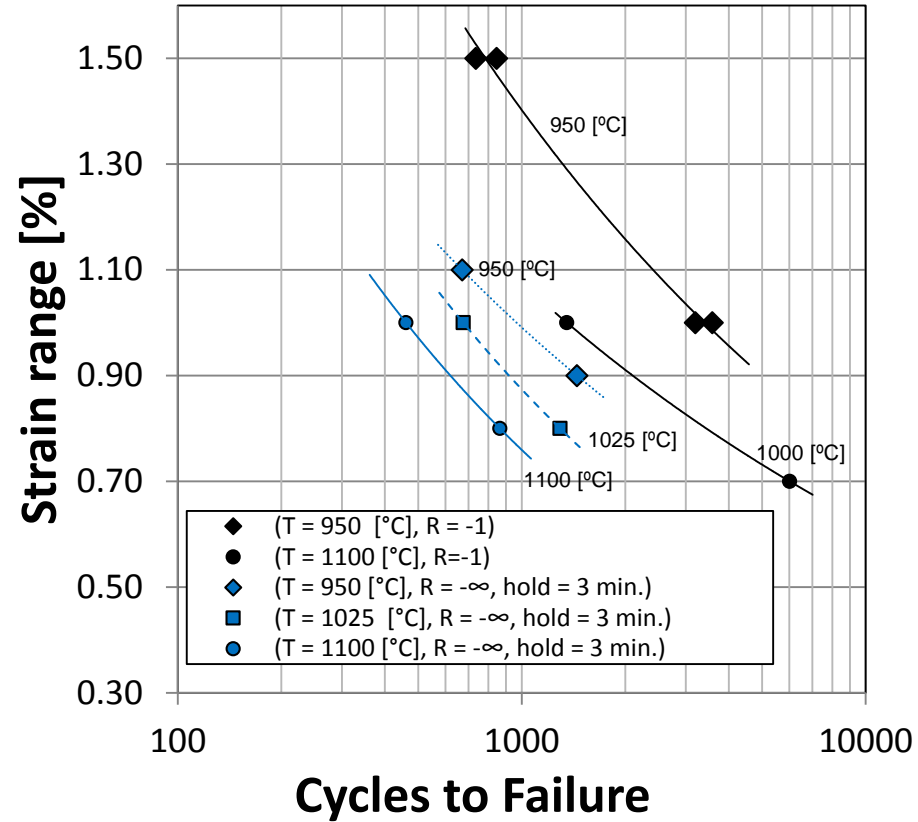
- Plastic strain range
- Environmental effects
- Influence of mean stress / stress range
- Creep damage (dwell)
- Microstructure / crystal orientation

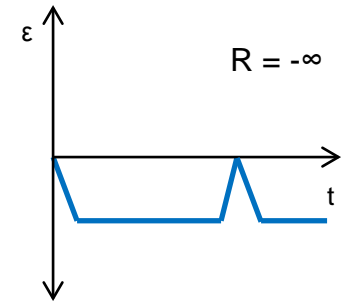
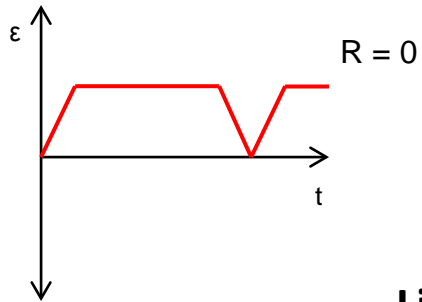


Effect of hold on LCF life: $R = 0$

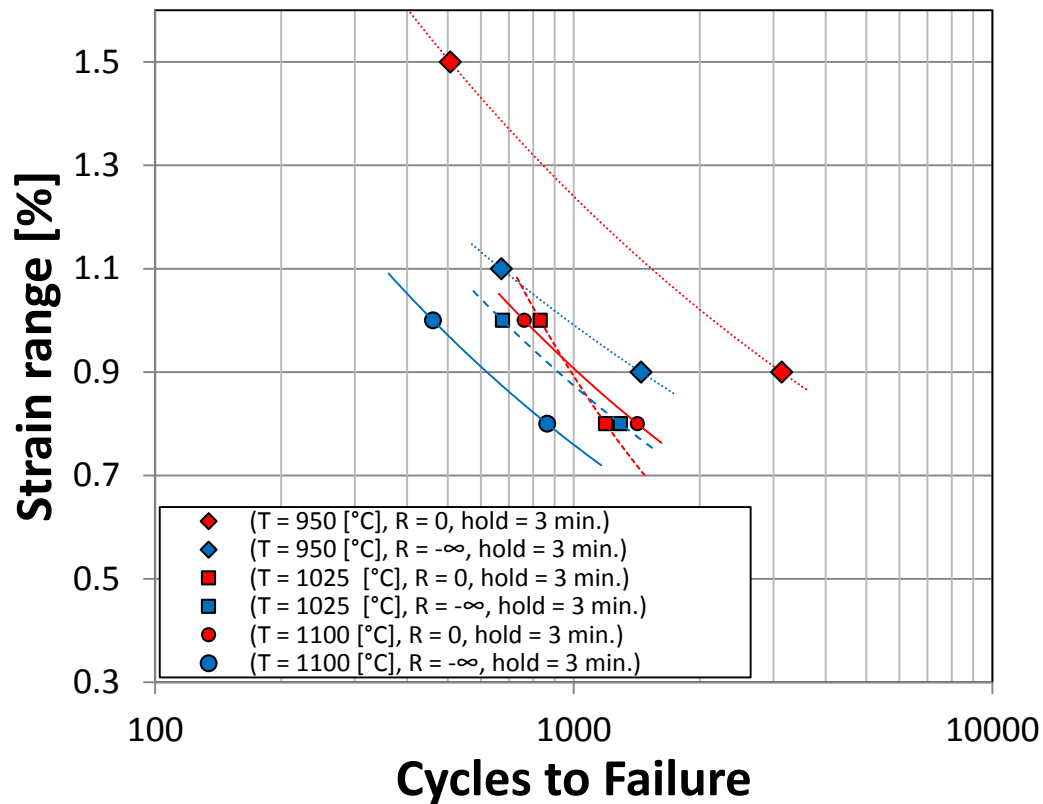


Effect of hold on LCF life: $R = -\infty$

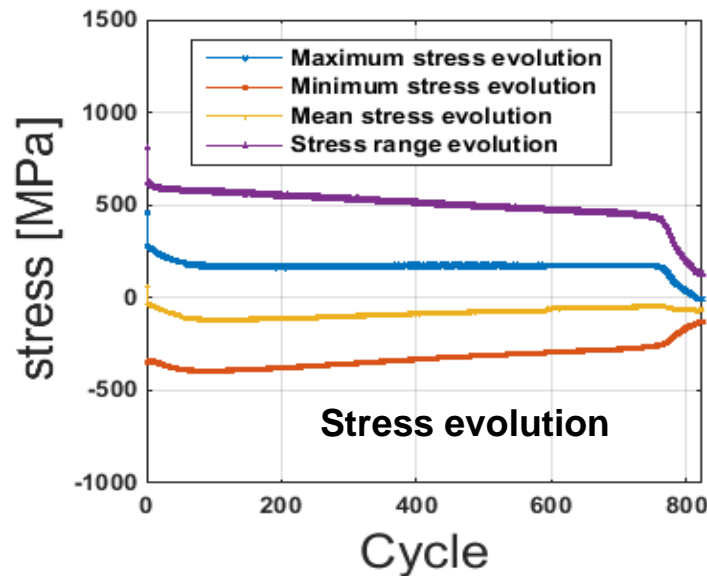
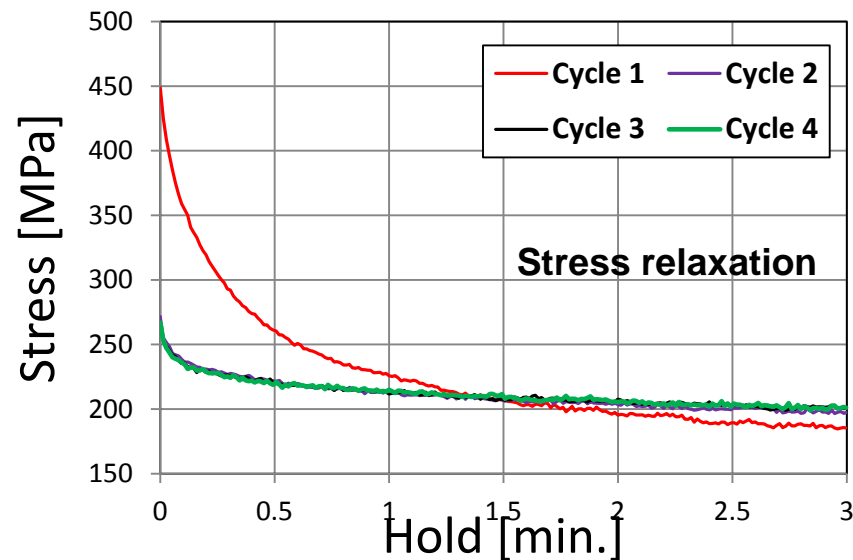
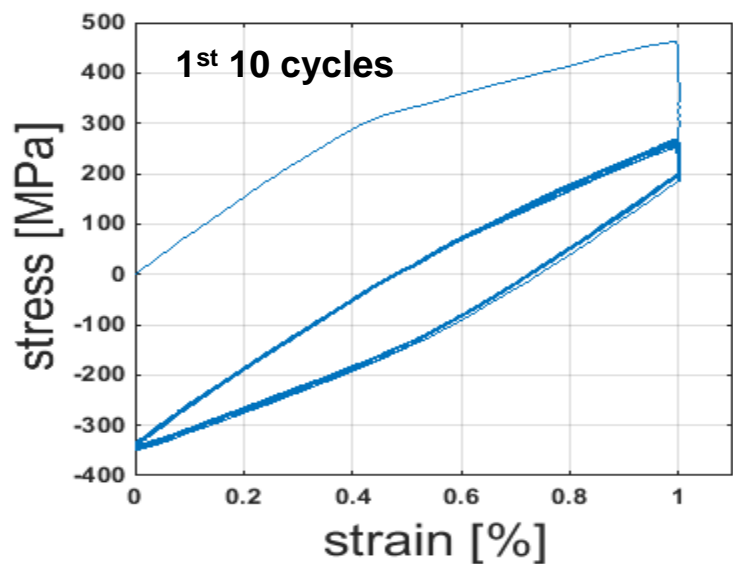




Life for low cycle creep-fatigue

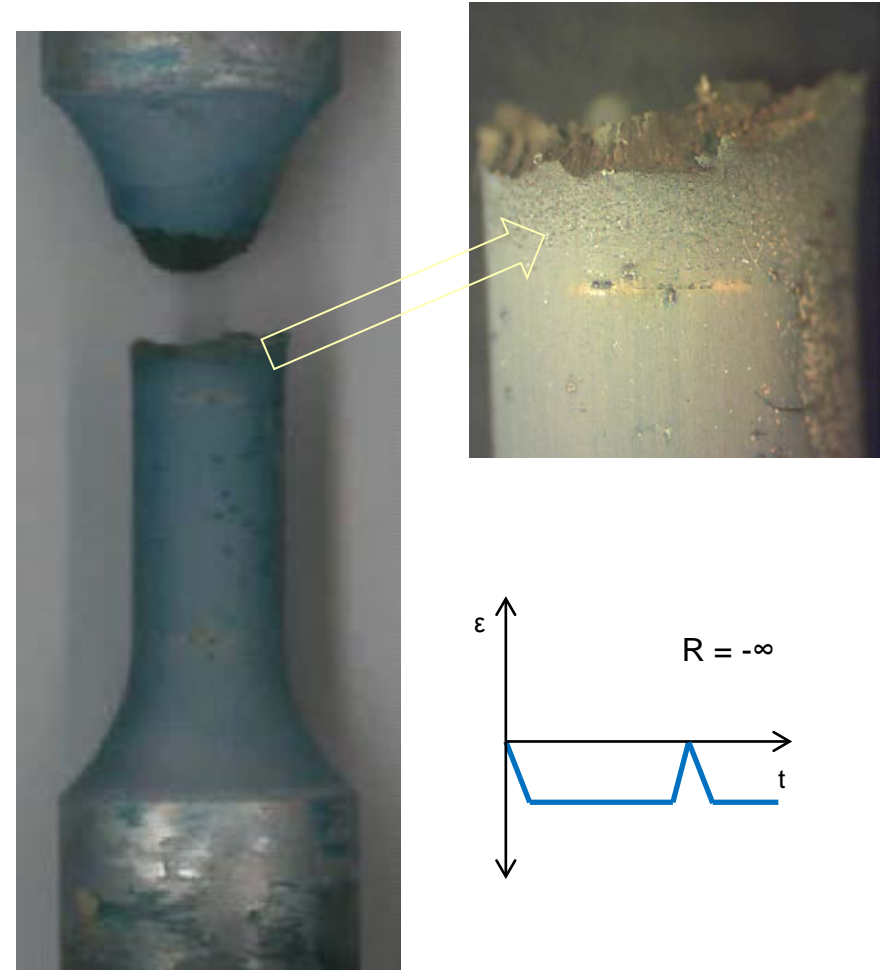
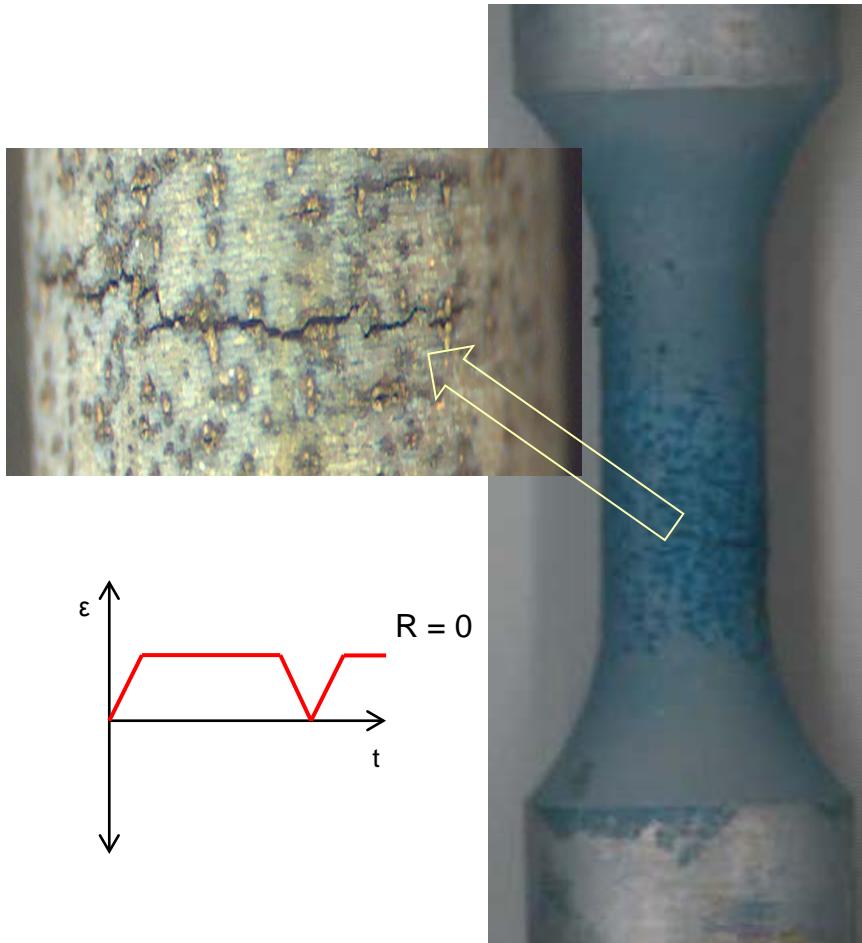


$T = 1100 \text{ }^\circ\text{C}$, $R = 0$, $\Delta\varepsilon = 1.0 \%$



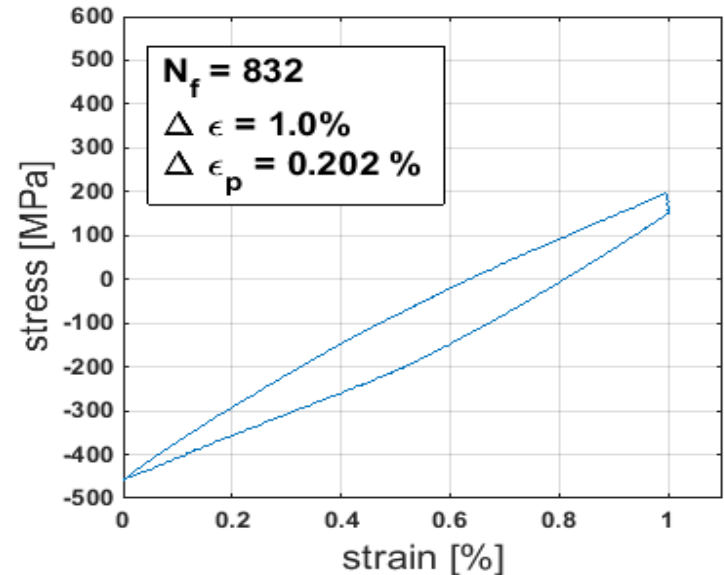
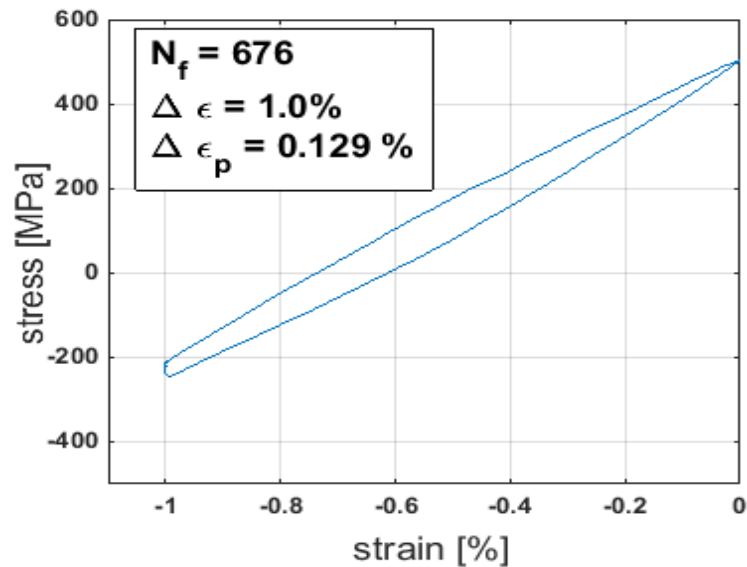
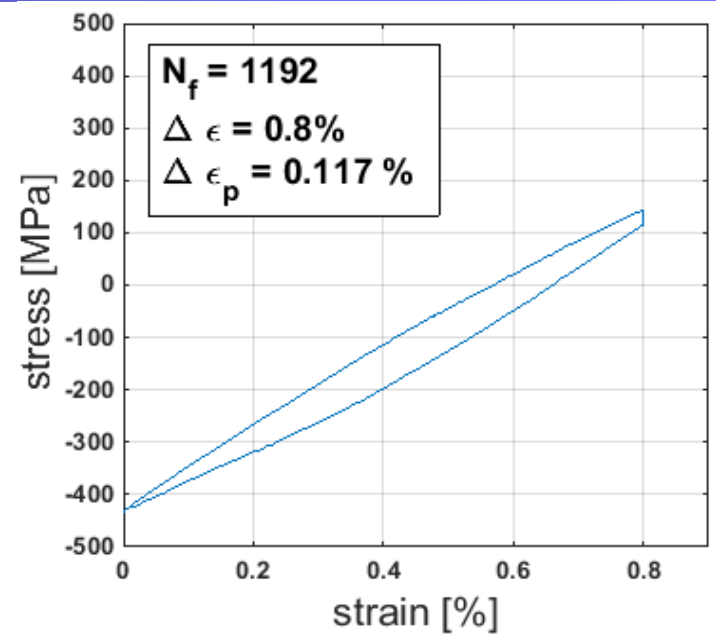
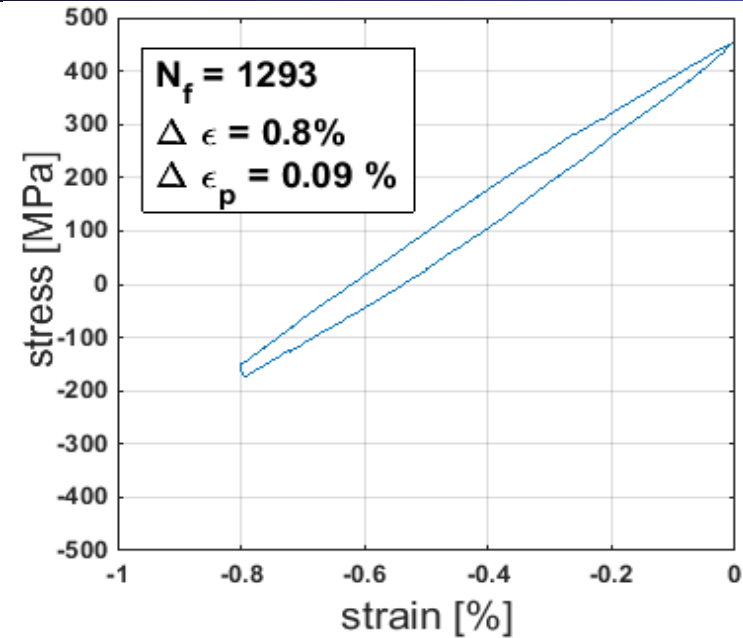
$R = 0, T = 1100^{\circ}\text{C}, \Delta\varepsilon = 0.8\%$
 $N_f = 1420$

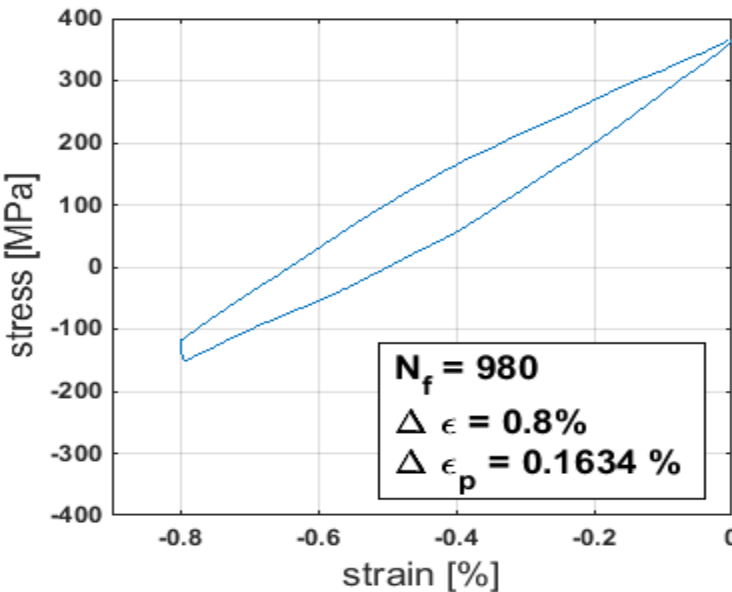
$R = -\infty, T = 1100^{\circ}\text{C}, \Delta\varepsilon = 0.8\%$
 $N_f = 980$



The George W. Woodruff School of Mechanical Engineering

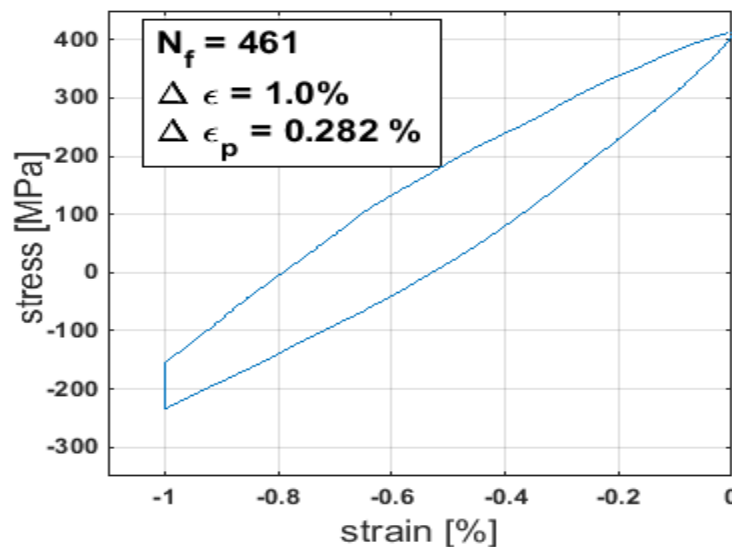
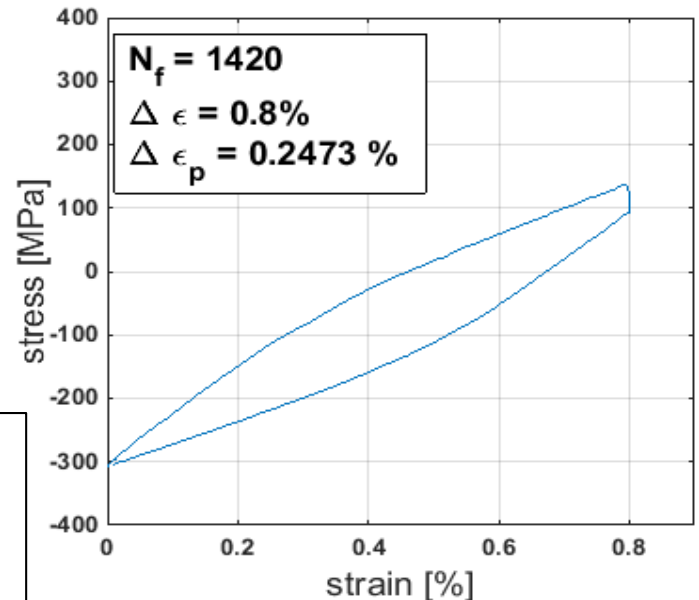
School of Materials Science and Engineering



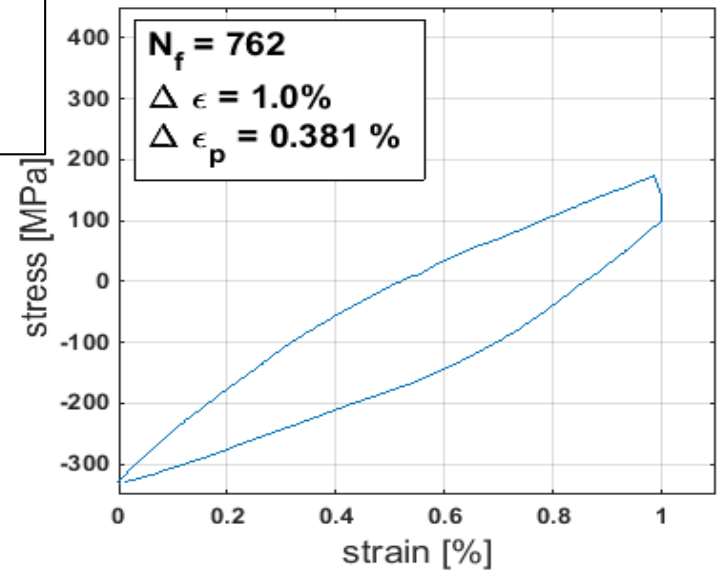


$\Delta \epsilon = 0.8\%$

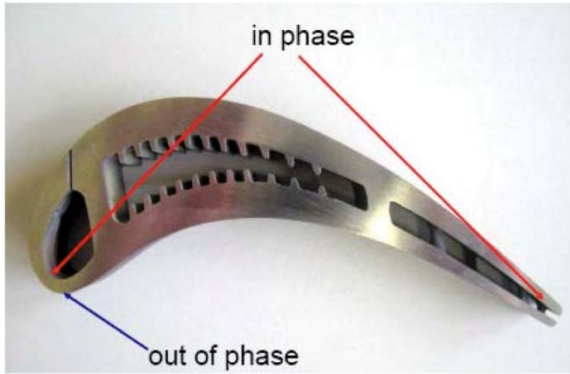
Plastic strain range alone does not explain life data at high temperatures. A Coffin-Manson relations would not be sufficient



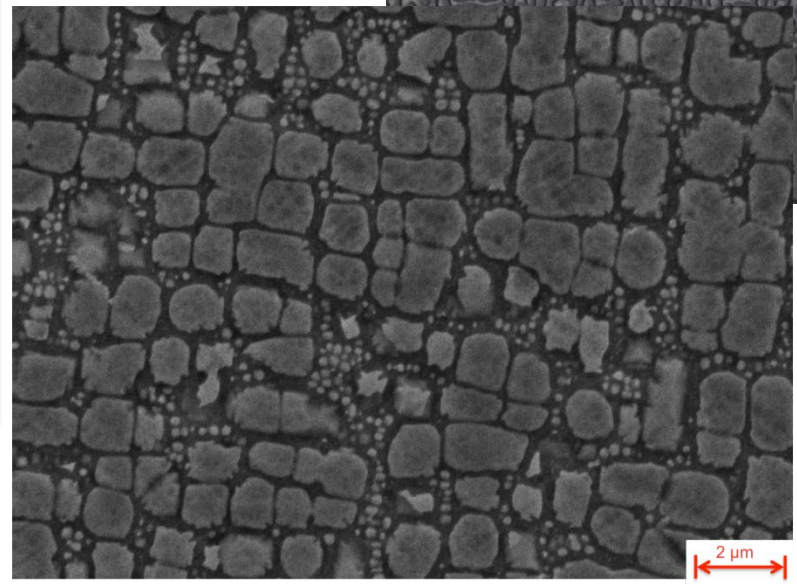
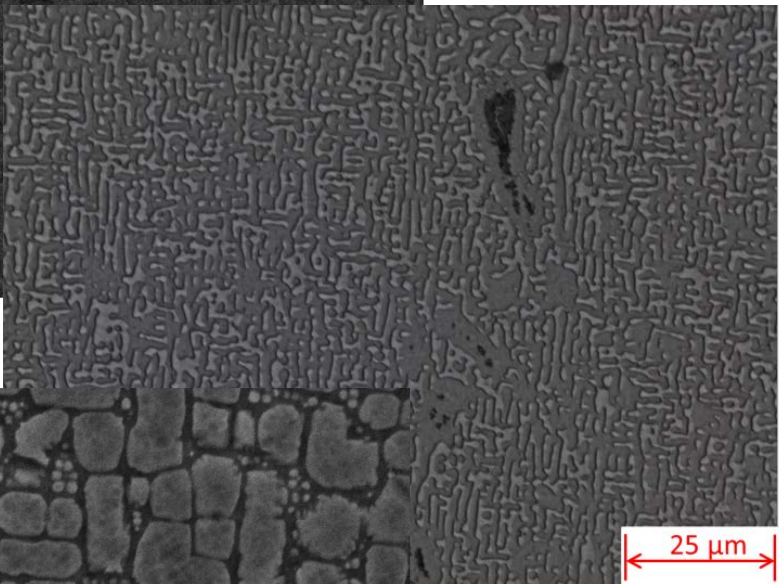
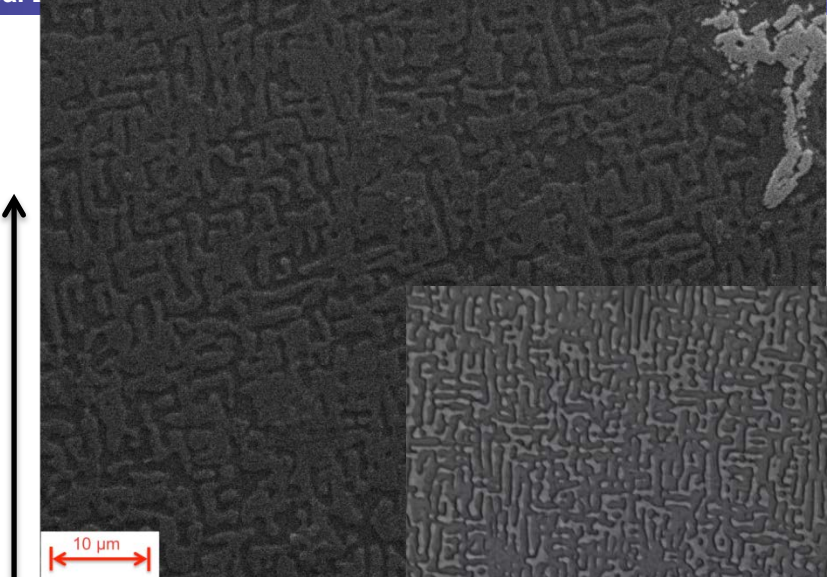
$\Delta \epsilon = 1.0\%$

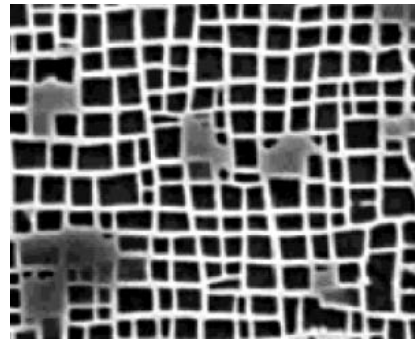


- Creep-fatigue interaction experiments on CMSX-8
- Influence of aging on microstructure and creep-fatigue interactions
- Microstructure-sensitive, temperature-dependent crystal viscoplasticity to capture the creep and cyclic deformation response



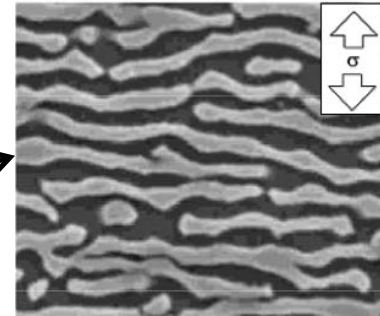
Distance from Root



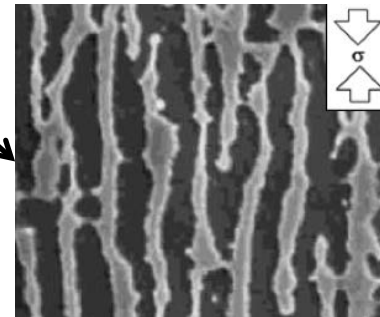


Tension

Compression

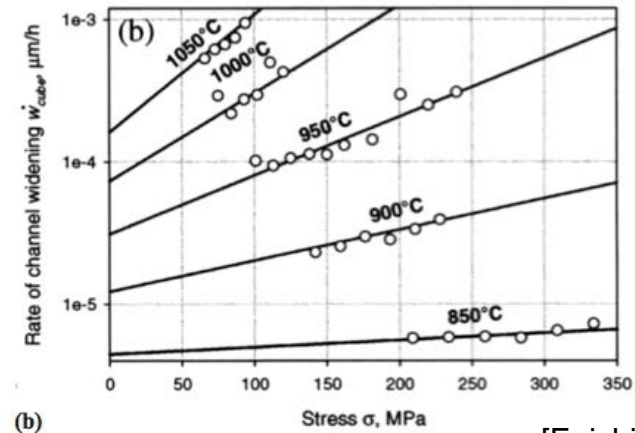
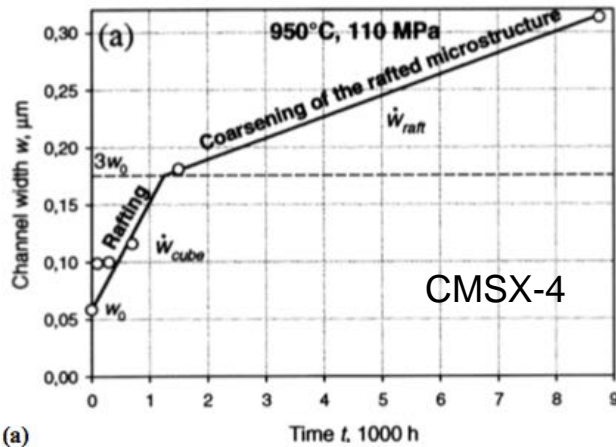


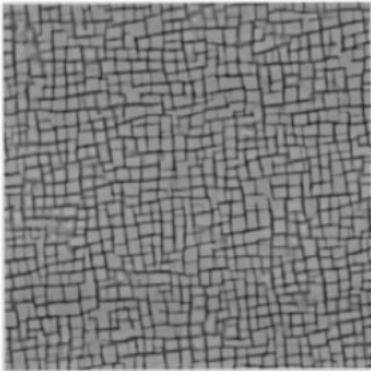
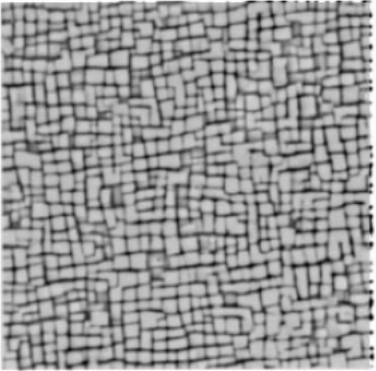
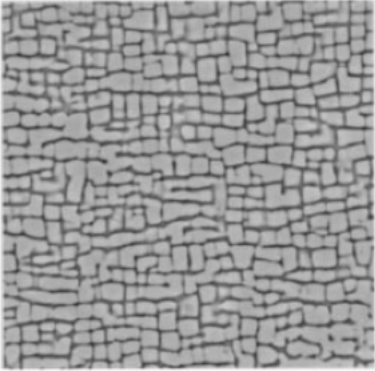
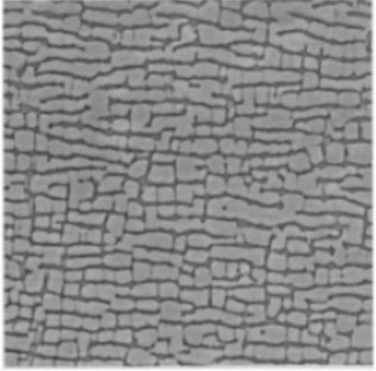
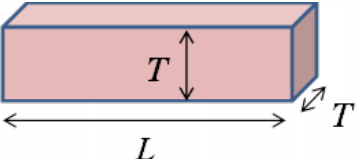
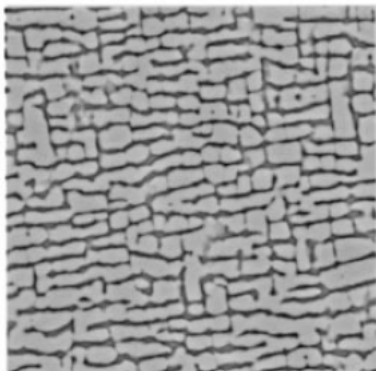
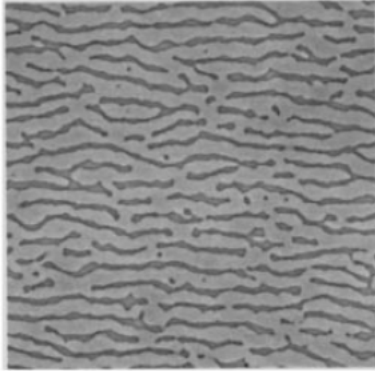
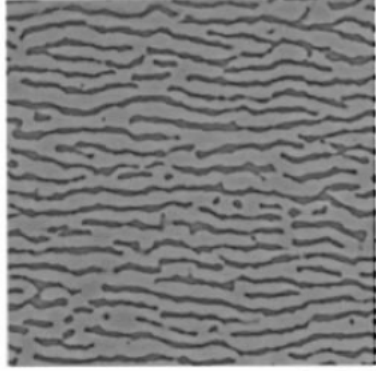
N-raft



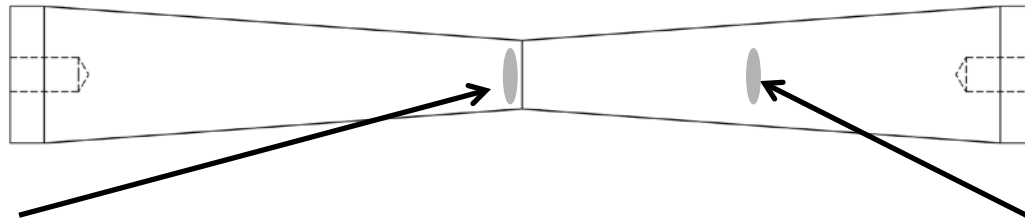
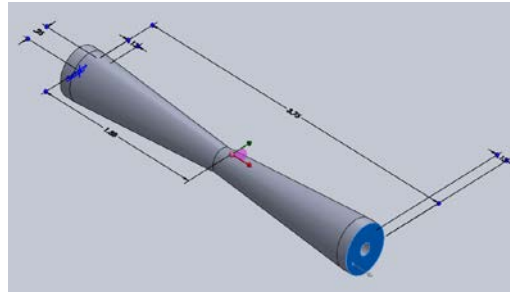
P-raft

$$\delta = \frac{2(a_{\gamma'} - a_{\gamma})}{a_{\gamma'} + a_{\gamma}}$$



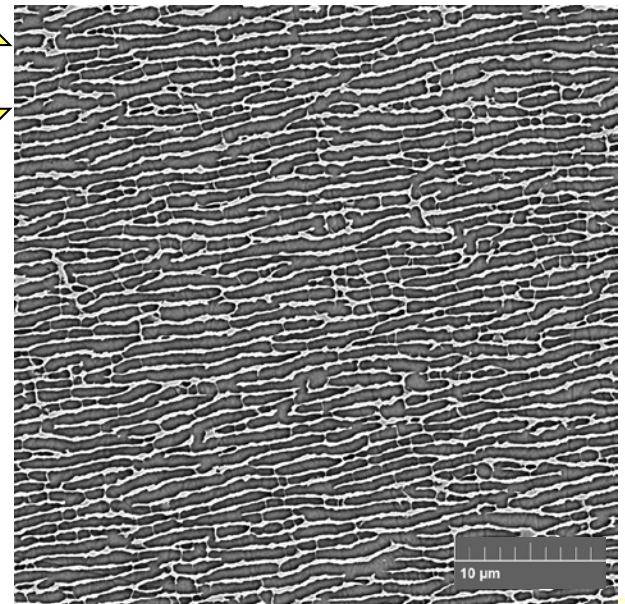
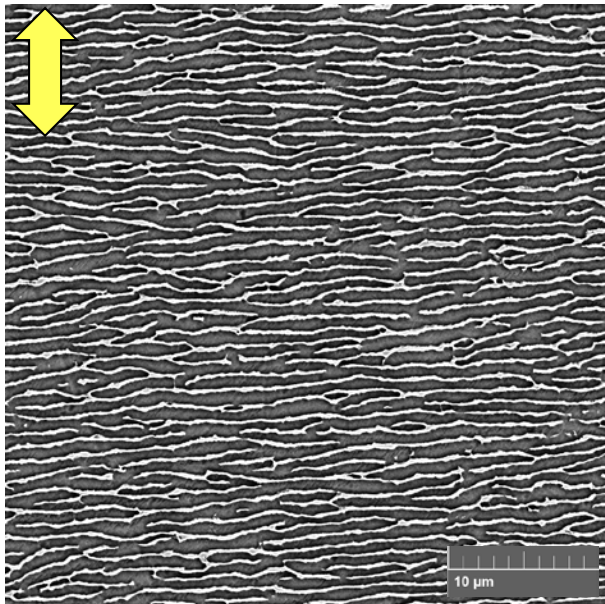
Initial	A: time=150 Hours strain=0.06% R=0.55	B: time=280 Hours strain=0.07% R=0.69	C: time=550 Hours strain=0.27% R=0.94
<p>CMSX-4</p> 			
	<p>D: time=695 Hours strain=0.13% R=1.07</p>	<p>E: time=1060 Hours strain=1.06% R=1.28</p>	<p>F: time=1170 Hours strain=0.83% R=1.39</p>
$R = \frac{L}{2T}$ 			

Objective: Obtain kinetic data to predict rafting and coarsening as a function of temperature, stress, microstructure and time

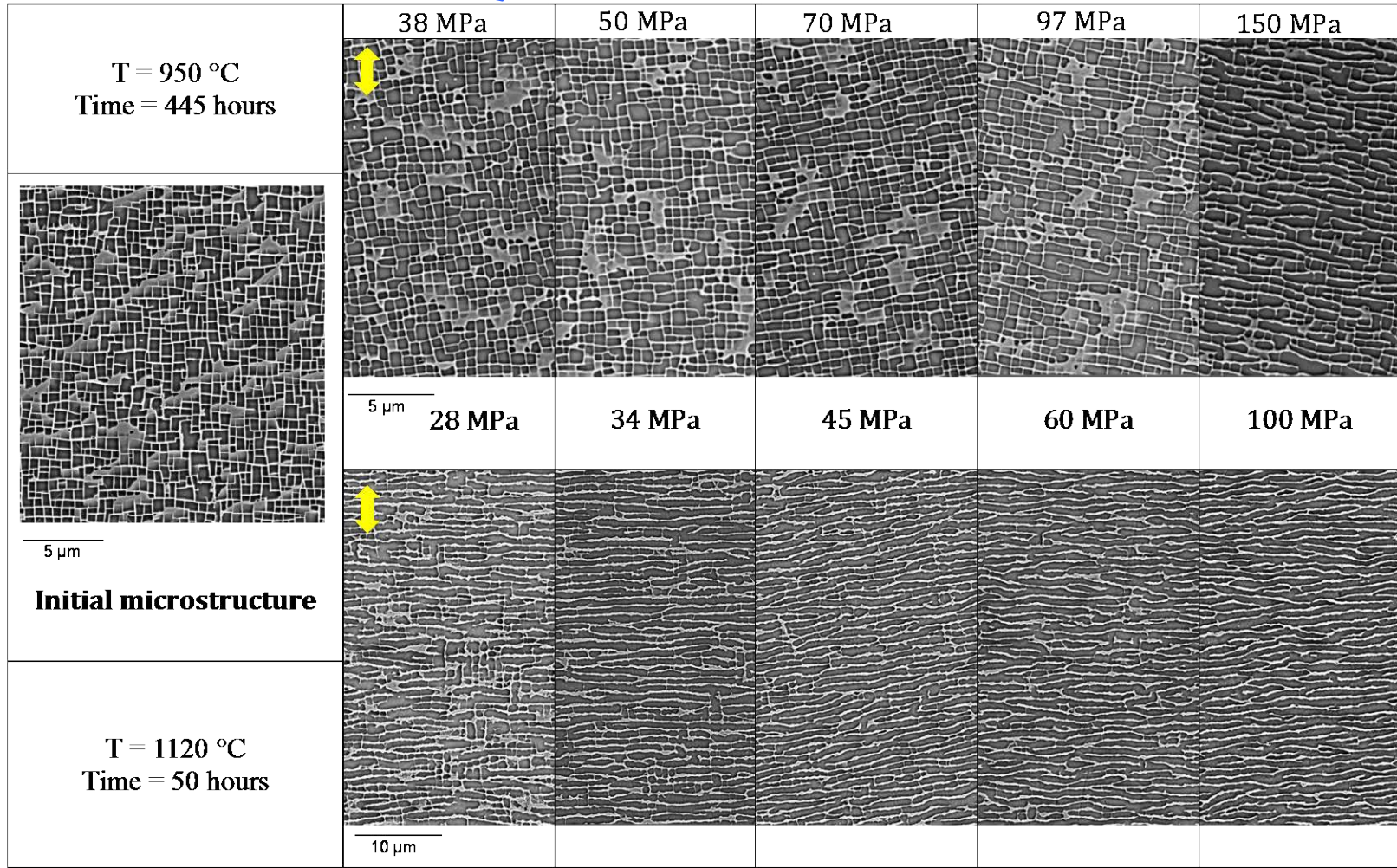
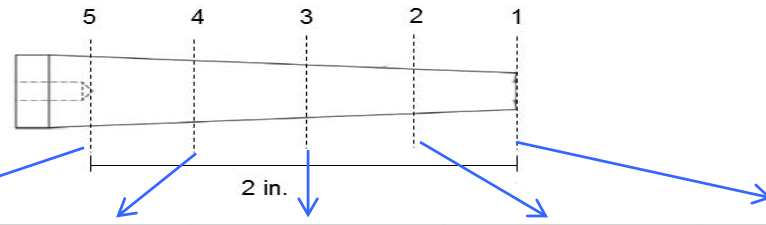


Fully Rafted
100 MPa

Partially Rafted
50 MPa



Test conditions
CMSX-8
Temperature: 1120° C
Force: 3.24kN
Time: 50 hrs



- 2-point correlation – A statistical representation of the microstructure that provides a magnitude measure in addition to the associated spatial correlation.

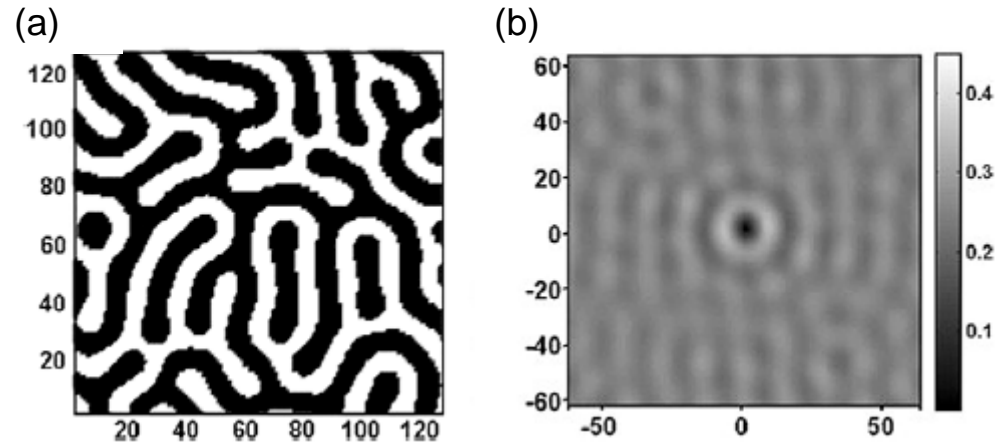
$$f(h, h' | \mathbf{r}) = \frac{1}{\text{vol}(\Omega)} \int_{\Omega} m(\mathbf{x}, h) m(\mathbf{x} + \mathbf{r}, h') d\mathbf{x}$$

$$\begin{aligned} {}^{np}F_{\mathbf{k}} &= \mathfrak{F}({}^{np}f_t) = \frac{1}{S} {}^nM_{\mathbf{k}}^* {}^pM_{\mathbf{k}} \\ &= \frac{1}{S} |{}^nM_{\mathbf{k}}| |{}^pM_{\mathbf{k}}| e^{-i {}^n\theta_{\mathbf{k}}} e^{i {}^p\theta_{\mathbf{k}}} \end{aligned}$$

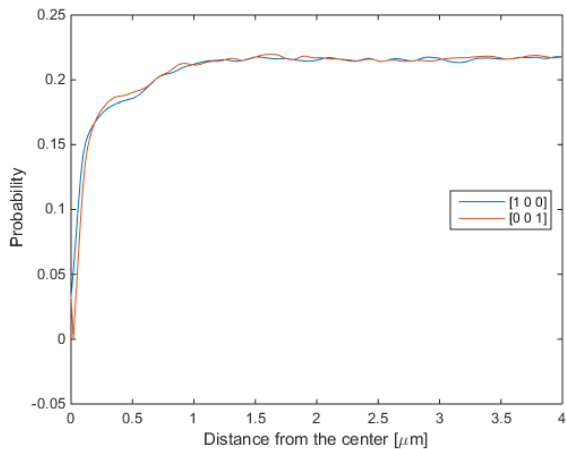
[Niezgoda, Fullwood and Kalidindi, 2008]

- 2-point correlations $f(h, h' | \mathbf{r})$ capture the probability density associated with finding an ordered pair of specific local state at the head and tail of a randomly placed vector \mathbf{r} into the microstructure.

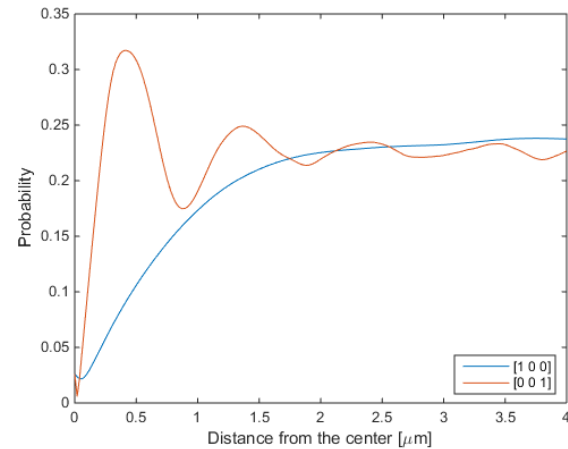
- **Cross-correlation**
Defined by $f(h, h' \neq h | \mathbf{r})$. The function gives the probability that a random vector of length x start in one phase and end in the other.



(a) An example of two phase microstructure (b) Cross-correlation for the black and white phases at the head and tail of a vector [Fullwood, Niezgoda, Adams, Kalidindi, 2010].

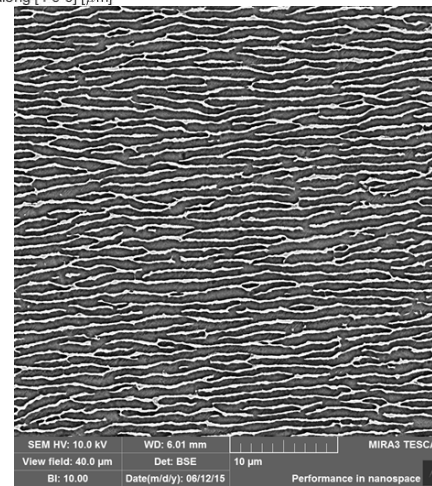
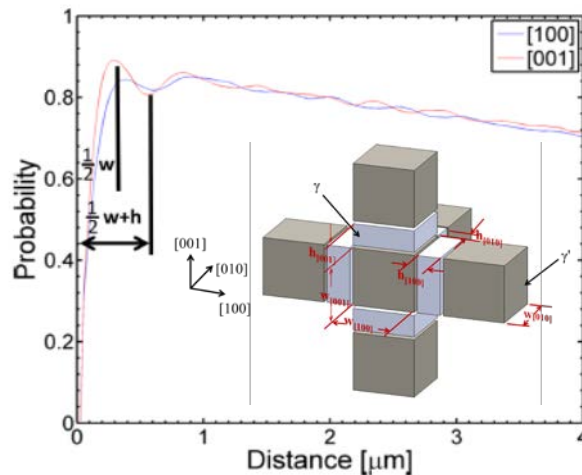
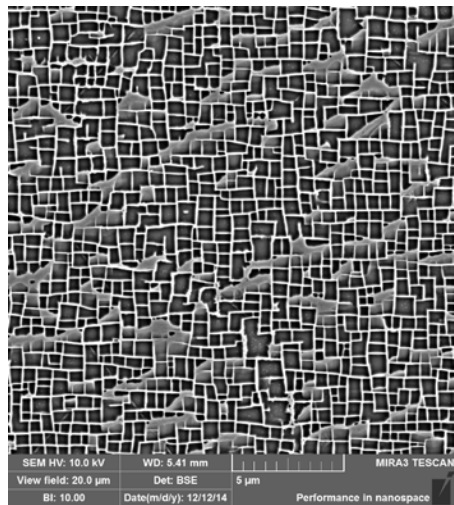
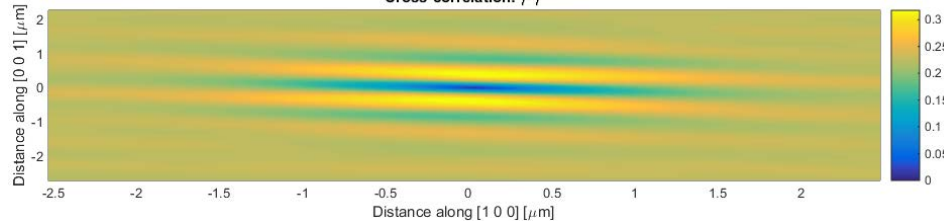
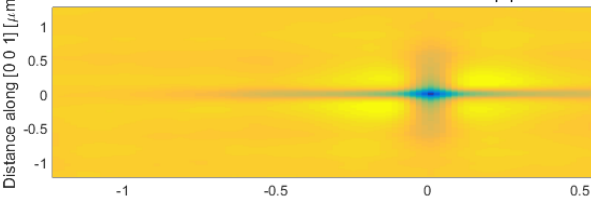


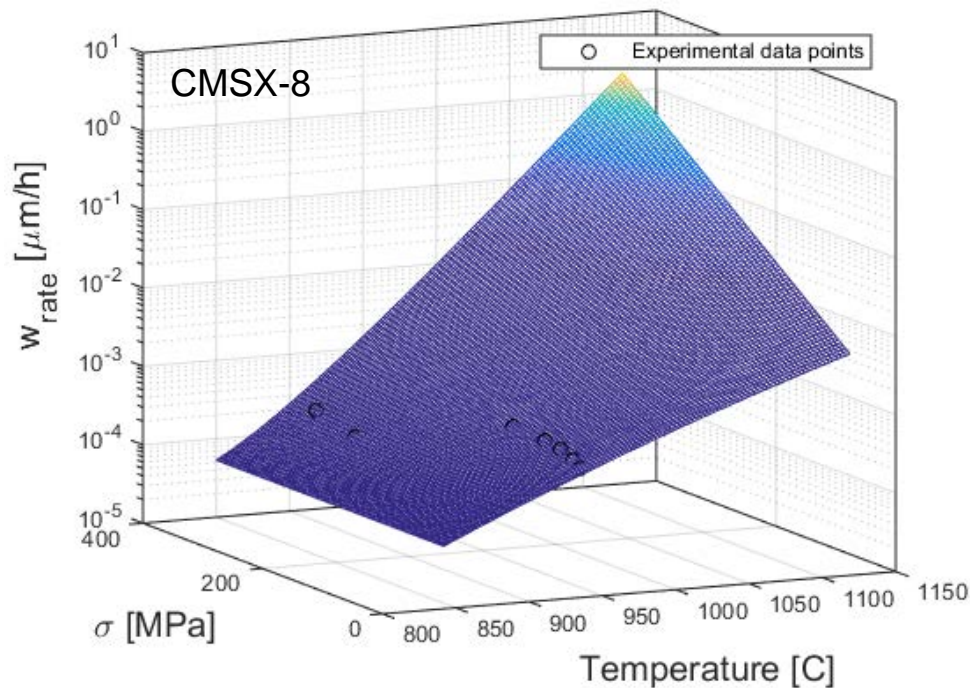
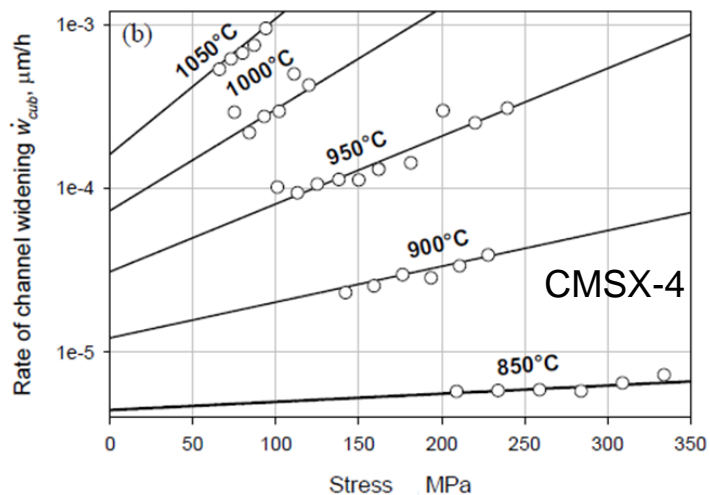
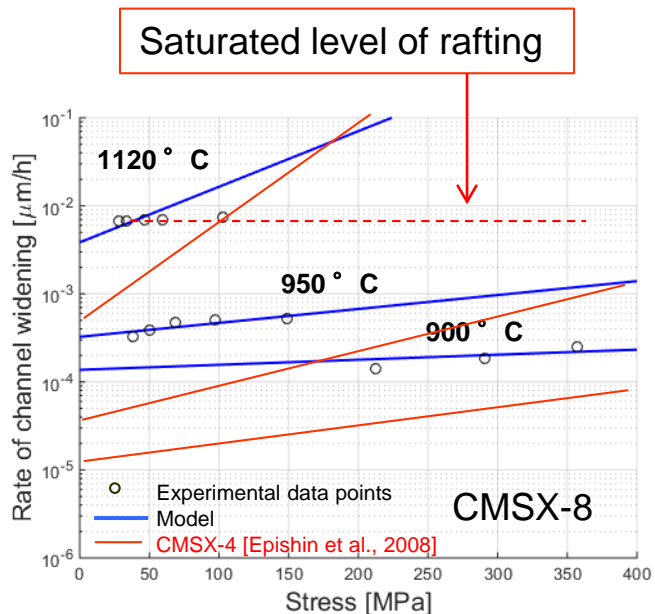
γ' precipitate and γ channel sizes are determined from the first peak and valley of the probabilistic curve of the corresponding micrograph.



Cross-correlation: $\gamma-\gamma'$

Cross-correlation: $\gamma-\gamma'$





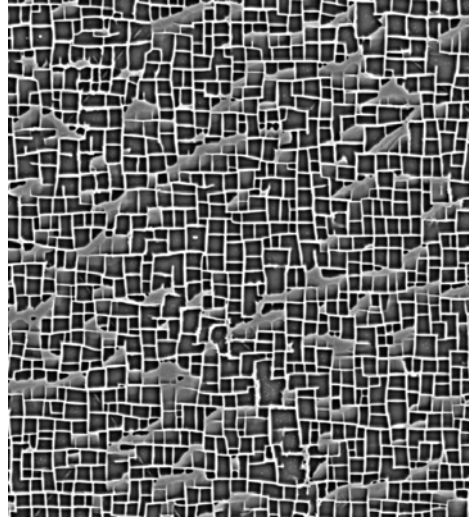
	A ($\mu\text{m/h}$)	Q (KJ/mol)	U_T (J/mol.Mpa.K ⁿ)	n
CMSX-8	2.0×10^5	205.80	0.033	1.525
CMSX-4	9.31×10^4	221.78	0.19	1.294

$$\dot{w}(T, \sigma) = A \cdot \exp\left[-\frac{Q - U(T) \cdot \sigma}{RT}\right]$$

$$U(T) = U_T(T - T_0)^n$$

[Epishin et al., 2008]

Initial Microstructure



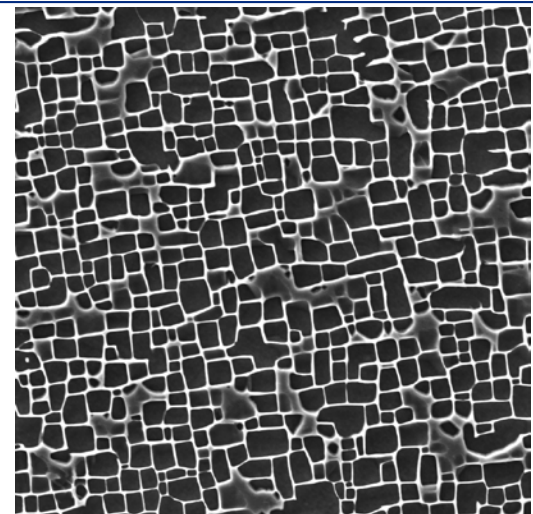
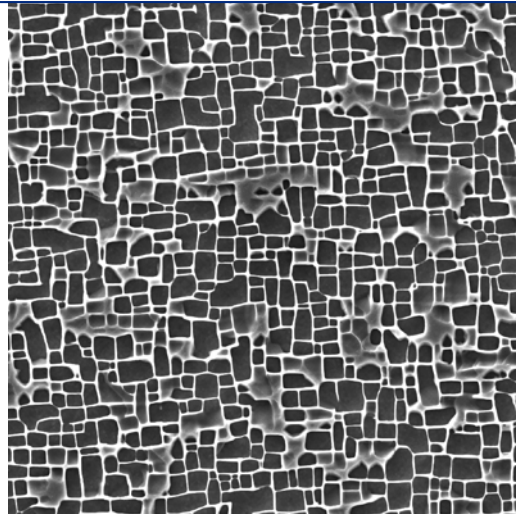
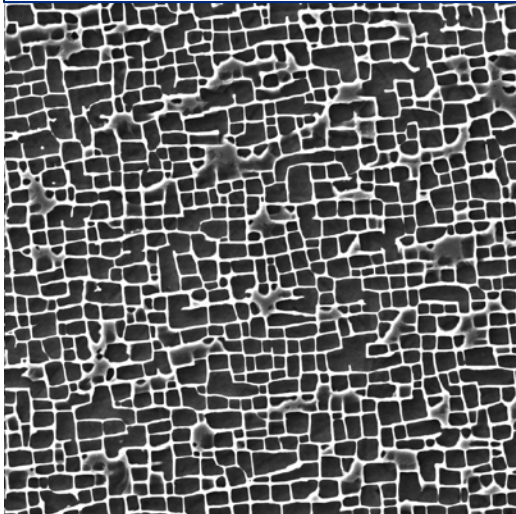
$\sigma = 0 \text{ Mpa}$
 $T = 950 \text{ }^\circ \text{C}$

5 μm

t = +400 hours

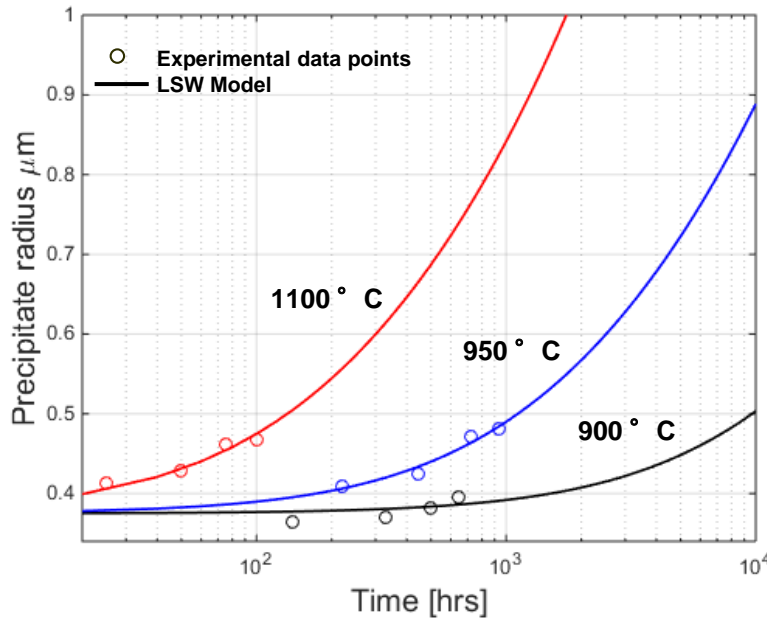
t = +700 hours

t = +900 hours



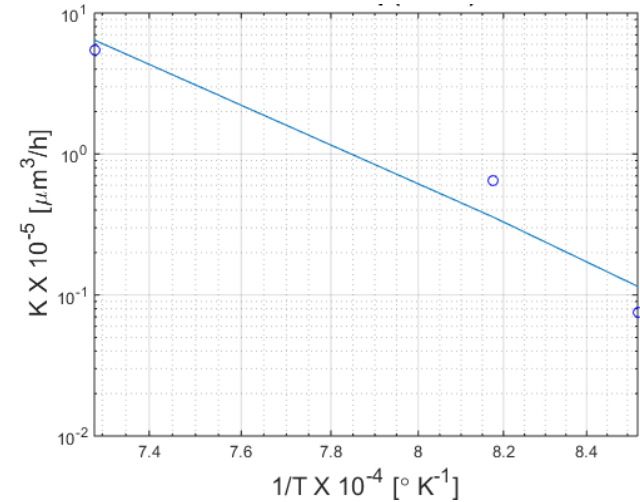
- According to Lifshitz-Slyozov-Wagner (LSW) theory particle coarsening process involves growth of the larger particles at the expense of the smaller ones to dissolve, with the driving force of reduction in interfacial energy of the system.
- Cube rate law indicates the volume diffusion

$$(r)^3 - (r_0)^3 = Kt \quad K = K_0 \exp\left(-\frac{Q_{coar}}{RT}\right)$$

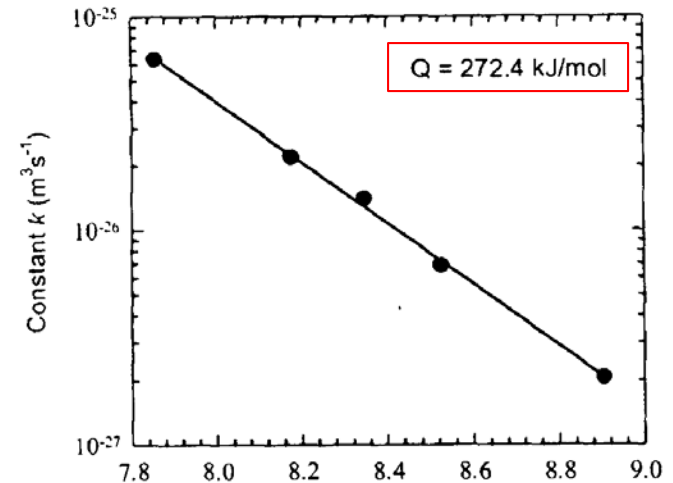


$$Q_{coar} (CMSX - 8) = 269.4 \text{ kJ/mol}$$

CMSX-8



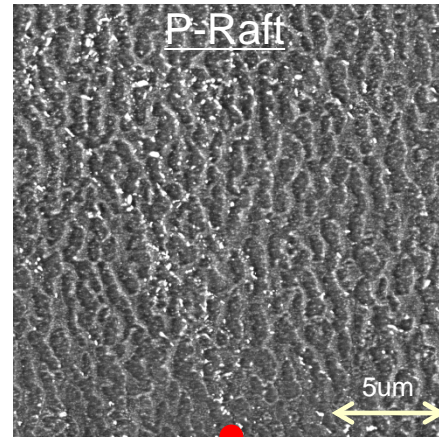
CMSX-4



Compression Creep Frame

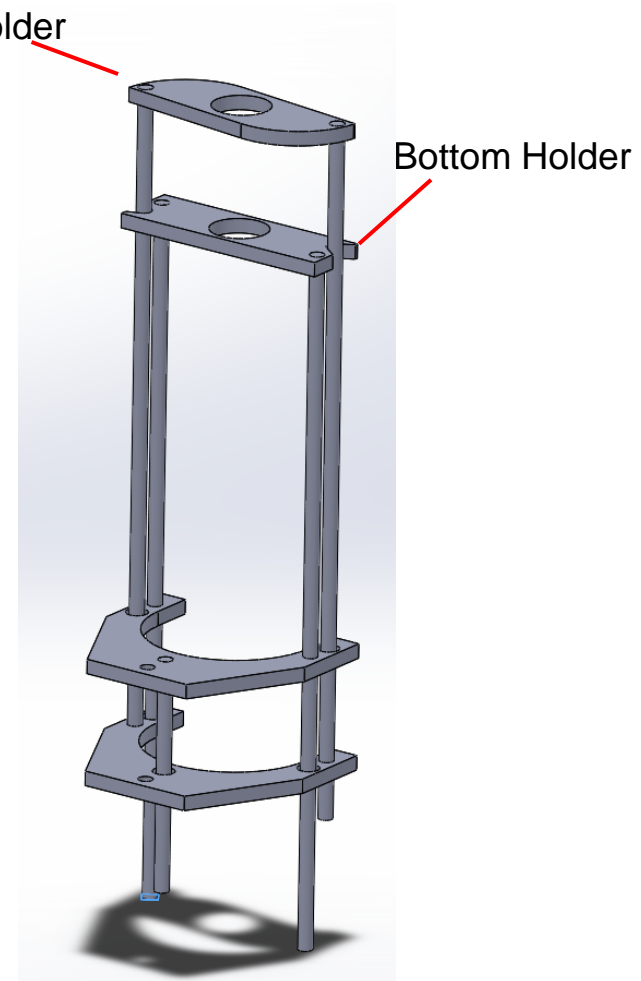


Ceramic Compression Creep Extensometer



Top Holder

Bottom Holder



Flux of all n components in CMSX-8 system during a diffusion controlled process can be described by the **effective diffusion coefficient**, D_{eff}

$$D_{eff} = D_{0,eff} \left(-\frac{Q_{eff}}{RT} \right)$$

$$Q_{eff} = \sum_{i=1}^n x_i Q_{Ni-i} \quad [\text{Ai et al., 2015}]$$

Prediction of Aging

Effective diffusion coefficient term embedded in LSW model of isotropic coarsening,

$$r^3 - r_o^3 = K(t - t_o)$$

$$K = \frac{64D_{eff}C_{\infty}\sigma\Omega^2}{9RT}$$

$$D_{eff} = D_{0,eff} \left(-\frac{Q_{eff}}{RT} \right)$$

Coarsening activation energy

Temperature-Dependent Constitutive Models

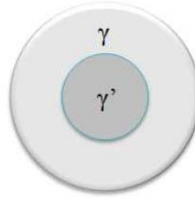
$$\dot{\gamma}^{\alpha} = \dot{\gamma}_0 \Theta(T) \left\langle \frac{\tau_v^{\alpha}}{D^{\alpha}} \right\rangle^n \exp \left\{ B_0 \left\langle \frac{\tau_v^{\alpha}}{D^{\alpha}} \right\rangle^{n+1} \right\} \text{sgn}(\tau^{\alpha} - \chi^{\alpha})$$

$$\Theta(T) = \exp\left(-\frac{Q_0}{RT}\right)$$

Composition dependent diffusivity parameter

Inter-diffusion coefficient of Ni-m binary system can be determined by DICTRA software

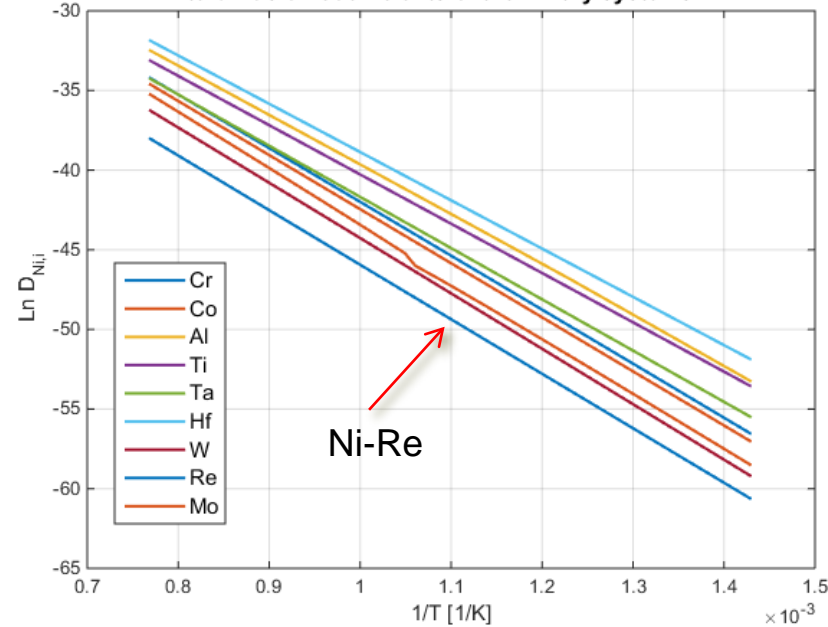
Equilibrium chemical composition of the γ phase is calculated at each temperature.



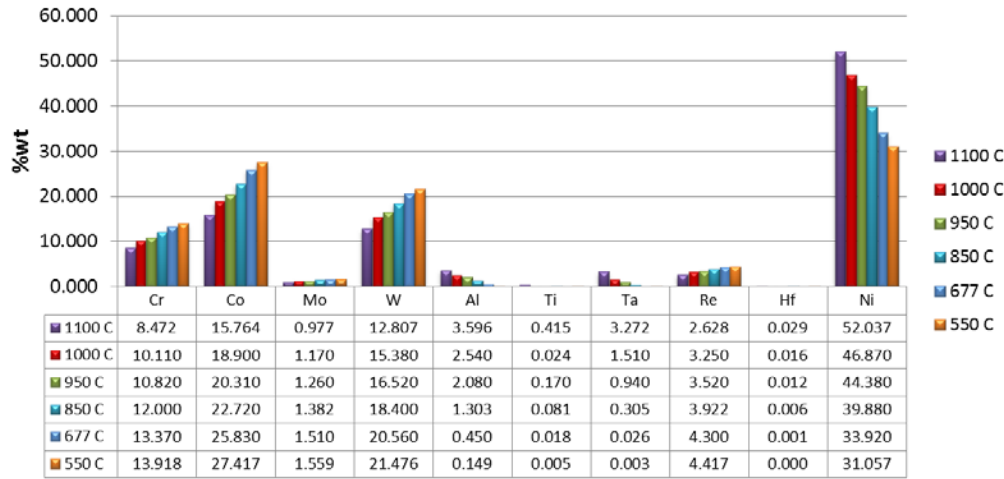
DICTRA
Databases:
TCNi5 / MOBNI2

$$D_{Ni-i} = D_{0,Ni-i} \left(-\frac{Q_{Ni-i}}{RT} \right)$$

Interdiffusion coefficients of the Binary systems Ni-i



γ Channel



Binary System	Ni-Cr	Ni-Co	Ni-Mo	Ni-W	Ni-Al	Ni-Ti	Ni-Ta	Ni-Re	Ni-Hf	Ni-Ni
$Q_{Ni,i}$ (KJ/mol)	2.81E+02	2.95E+02	2.82E+02	2.89E+02	2.60E+02	2.57E+02	2.67E+02	2.85E+02	2.52E+02	2.67E+02
$D_{0,Ni,i}$ (m ² /s)	2.75E-04	3.35E-04	2.02E-04	7.23E-05	5.18E-05	8.86E-05	7.23E-05	8.27E-06	1.91E-04	7.25E-08
X_i	1.27E-01	2.10E-01	7.97E-03	5.47E-02	6.15E-02	3.28E-04	5.45E-03	1.14E-02	5.86E-05	5.22E-01
$X_i Q_{Ni,i}$	3.57E+01	6.18E+01	2.25E+00	1.58E+01	1.60E+01	8.43E-02	1.46E+00	3.25E+00	1.48E-02	1.40E+02

$$Q_{eff} = \sum_{i=1}^n x_i Q_{Ni-i}$$

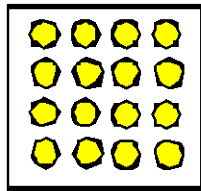
Effective Activation energy /
Coarsening Activation energy

= 275.89 kJ/mol

The influence of perturbations in composition on aging and diffusion-controlled processes is feasible with this methodology.

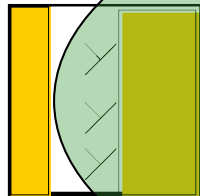
- Creep-fatigue interaction experiments on CMSX-8
- Influence of aging on microstructure and creep-fatigue interactions
- **Microstructure-sensitive, temperature-dependent crystal viscoplasticity to capture the creep and cyclic deformation response**

Atomic
(Interfaces,
Cores, Partials)



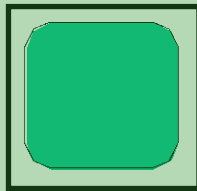
$O(10^{-10} \text{ m})$

Channel
Dislocations



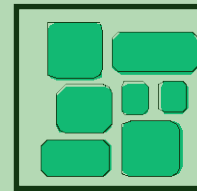
$O(10^{-8} \text{ m})$

Precipitates



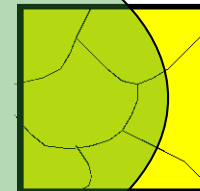
$O(10^{-7} \text{ m})$

Collections of
Precipitates;
GB cracks

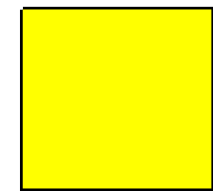


$O(10^{-6} \text{ m})$

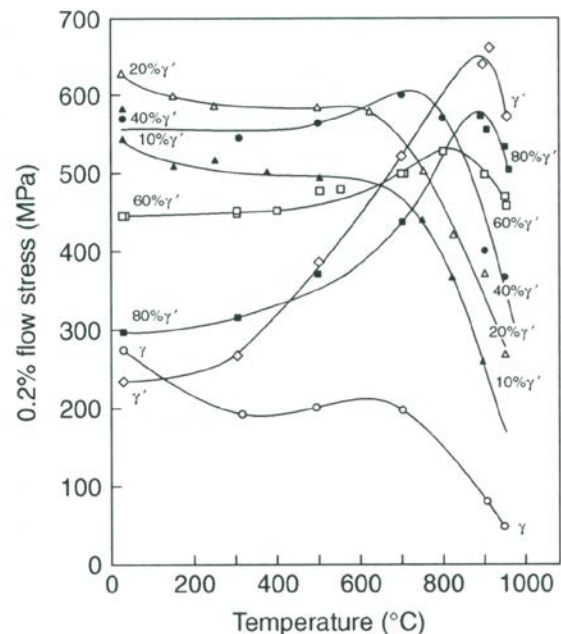
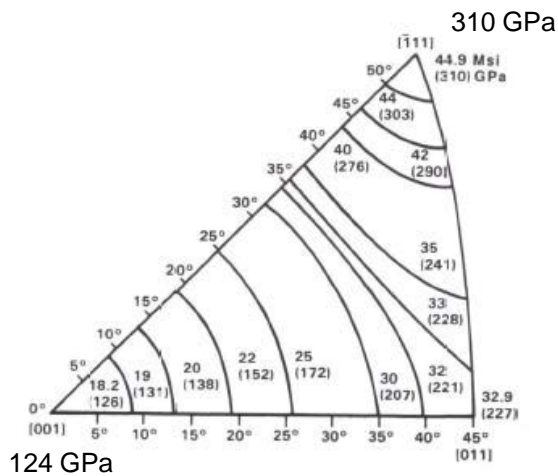
Shear bands
Grains



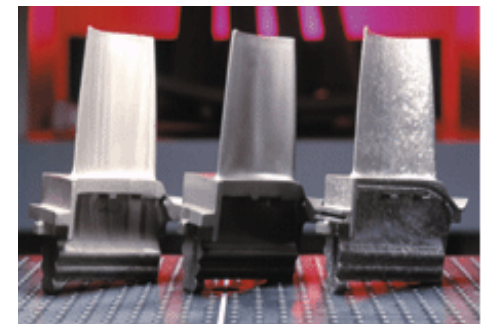
$O(10^{-5} \text{ m})$



[Shenoy, Tjipowidjojo, and McDowell, 2008]



[Reed, 2008]



components

Kinematic relations including temperature dependence

Deformation gradient

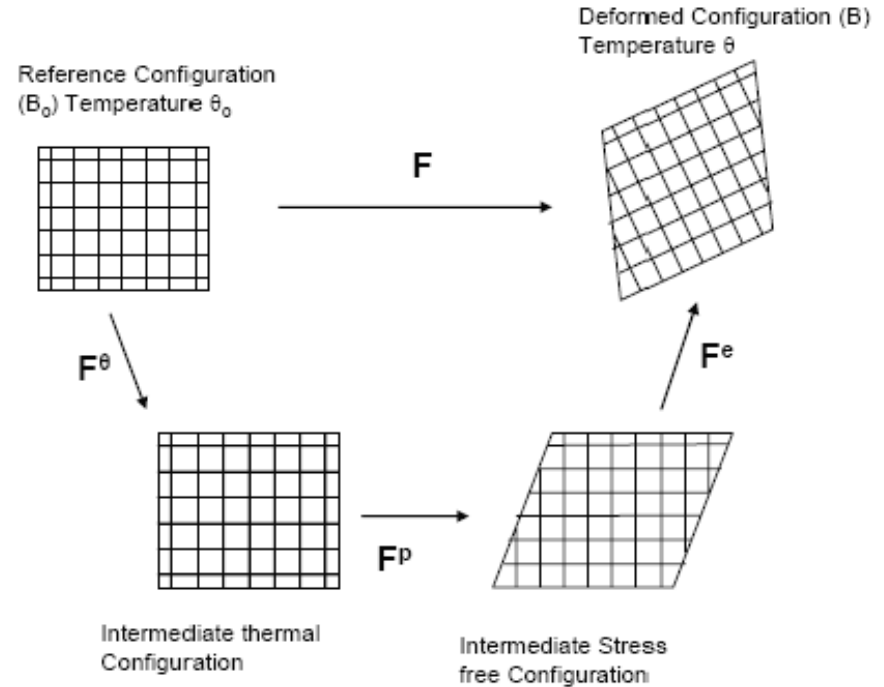
$$\mathbf{F} = \frac{\partial \mathbf{x}}{\partial \mathbf{X}} = \mathbf{F}^e \cdot \mathbf{F}^p \cdot \mathbf{F}^\theta$$

Velocity gradient

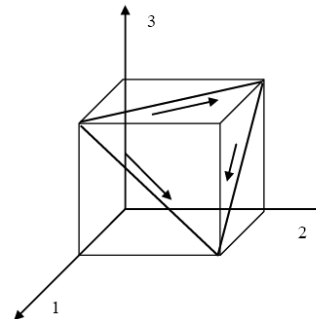
$$\mathbf{L} = \dot{\mathbf{F}} \cdot \mathbf{F}^{-1}$$

Macroscopic plastic velocity gradient

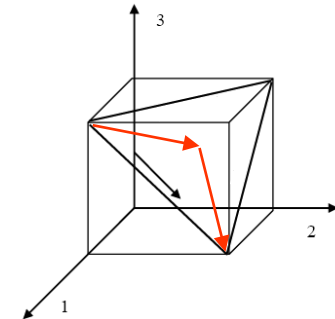
$$\mathbf{L}^p = \dot{\mathbf{F}}^p \mathbf{F}^{p-1} = \sum_{\alpha=1}^{N_{slip}} \dot{\gamma}^{(\alpha)} \left(\mathbf{s}_o^{(\alpha)} \otimes \mathbf{n}_o^{(\alpha)} \right)$$



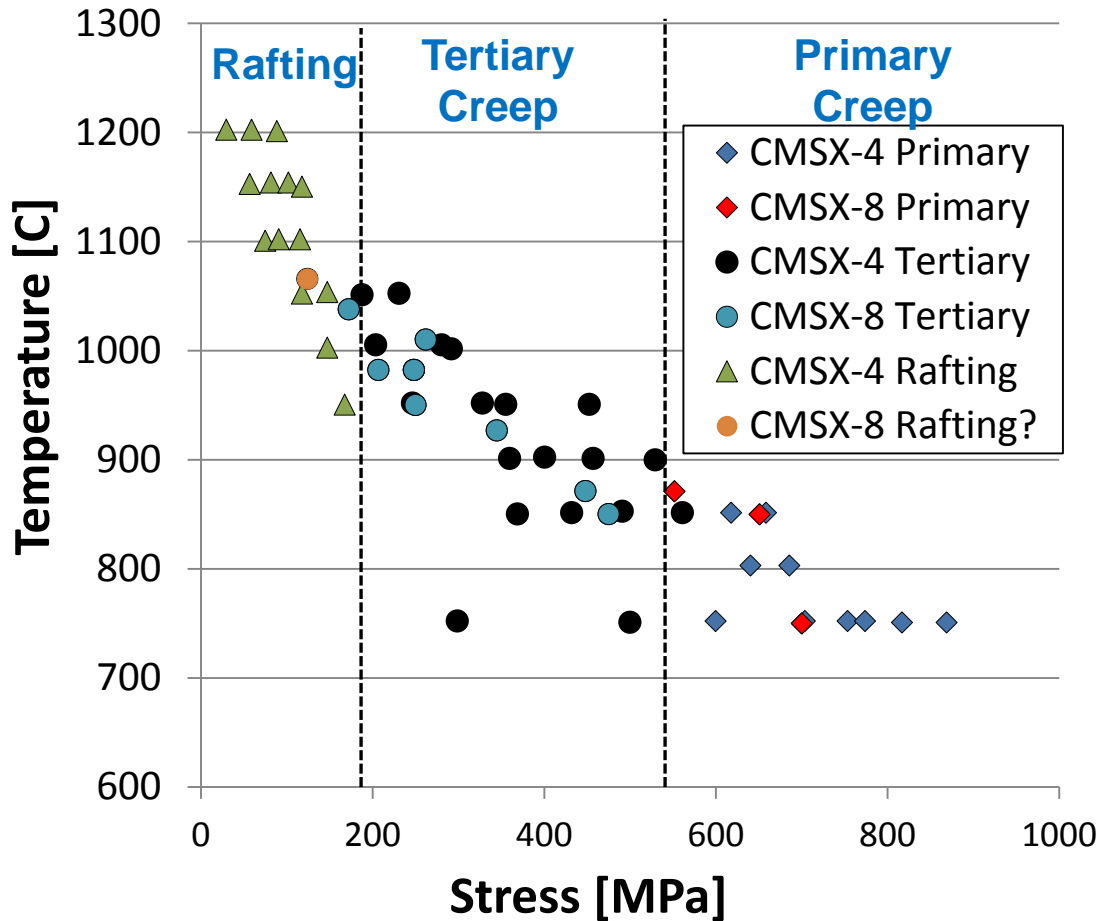
In γ : 12 octahedral slip systems active



In γ' : 12 octahedral slip systems moving as dislocation ribbons

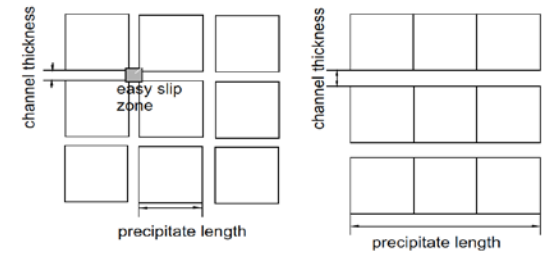


Influence of stress and temperature on modes of creep deformation



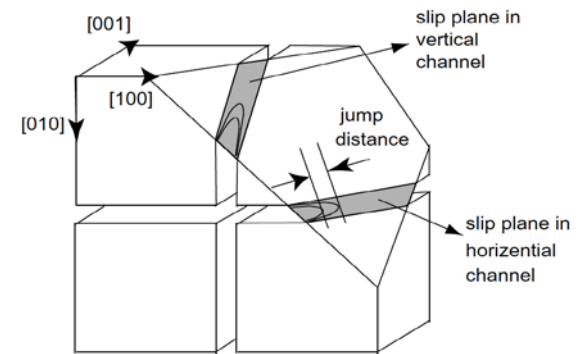
[Reed, 2006; Ma, Dye, and Reed, 2008, CMSX-8 Data]

Rafting – transport of matter constituting the γ phase out of the vertical channels and into the horizontal ones (tensile creep case)



[Ma, Dye, and Reed, 2008]

Tertiary – dislocation activity restricted to $a/2\langle 110 \rangle$ form operating on $\{111\}$ slip planes in the γ channels



[Ma, Dye, and Reed, 2008]

Primary – γ' particles are sheared by dislocation ribbons of overall Burgers vector $a\langle 112 \rangle$ dissociated into superlattice partial dislocations separated by a stacking fault; shear stress must above threshold stress (about 550 MPa)

Inelastic Velocity Gradient

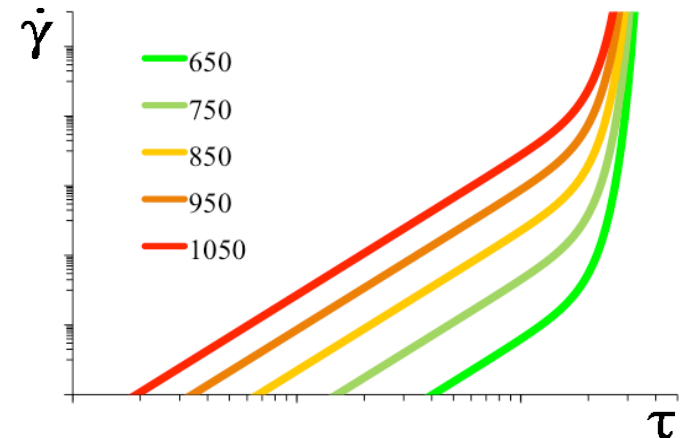
$$\mathbf{L}^{in} = \dot{\mathbf{F}}^{in} \mathbf{F}^{in-1} = f_{\gamma} \left(\sum_{\alpha=1}^{12} \dot{\gamma}_{\gamma}^{in(\alpha)} \left(\hat{\mathbf{d}}^{(\alpha)} \otimes \hat{\mathbf{n}}^{(\alpha)} \right) \right) + f_{\gamma'} \left(\sum_{\alpha=13}^{24} \dot{\gamma}_{L1_2}^{in(\alpha)} \left(\hat{\mathbf{d}}^{(\alpha)} \otimes \hat{\mathbf{n}}^{(\alpha)} \right) \right)$$

Inelastic Shear Strain Rate

$$\left\{ \begin{aligned} \dot{\gamma}_{\gamma}^{in(\alpha)} &= \rho_{\gamma}^{(\alpha)} b \lambda_{\gamma}^{(\alpha)} F_{attack} \text{sign} \left(\tau^{(\alpha)} + \tau_{mis}^{(\alpha)} - \chi^{(\alpha)} \right) \exp \left\{ \frac{-Q_{slip}^{110} + \left(\left| \tau^{(\alpha)} + \tau_{mis}^{(\alpha)} - \chi^{(\alpha)} \right| - \tau_{\gamma pass}^{(\alpha)} - \tau_{oro}^{(\alpha)} \right) V_{c1}^{(\alpha)}}{kT} \right\} \\ \dot{\gamma}_{L1_2}^{in(\alpha)} &= \rho_{L1_2}^{(\alpha)} b \lambda_{L1_2}^{(\alpha)} F_{attack} \text{sign} \left(\tau^{(\alpha)} - \chi^{(\alpha)} \right) \exp \left\{ \frac{-Q_{slip}^{112} + \left(\left| \tau^{(\alpha)} - \chi^{(\alpha)} \right| - \tau_{L1_2 pass}^{(\alpha)} - \tau_{APB} \right) V_{c2}^{(\alpha)}}{kT} \right\} \end{aligned} \right.$$

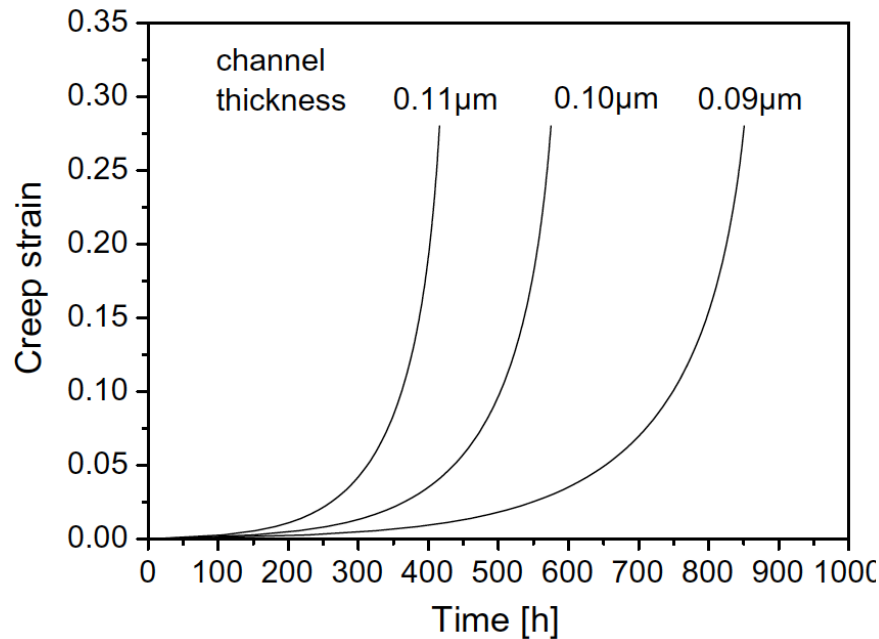
Evolution Equations

$$\left\{ \begin{aligned} \dot{\rho}_{\gamma}^{(\alpha)} &= \frac{1}{b} \left(\frac{c_{mult1}}{\lambda_{\gamma}^{(\alpha)}} - c_{annh1} \rho_{\gamma}^{(\alpha)} \right) \left| \dot{\gamma}_{\gamma}^{in(\alpha)} \right| \\ \dot{\rho}_{L1_2}^{(\alpha)} &= c_{mult21} \rho_{pb}^{(\alpha)} \Gamma + \frac{c_{mult22}}{b \lambda_{\gamma'}^{(\alpha)}} \left| \dot{\gamma}_{\gamma'}^{(\alpha)} \right| - c_{annh2} \rho_{\gamma'}^{(\alpha)} \left| \dot{\gamma}_{\gamma'}^{(\alpha)} \right| \\ \dot{\rho}_{pb}^{(\alpha)} &= \frac{c_{mult}^{pb}}{b L_{\gamma}} \left| \dot{\gamma}_{\gamma}^{in(\alpha)} \right| - c_{annh}^{pb} \rho_{pb}^{(\alpha)} \left| \dot{\gamma}_{\gamma}^{in(\alpha)} \right| \end{aligned} \right.$$

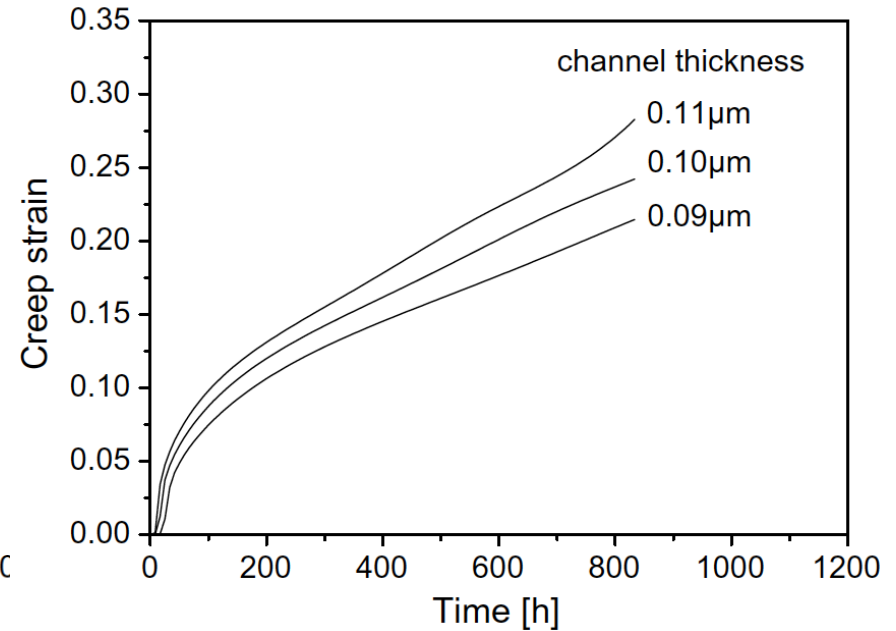


CMSX-4 Model Predictions

Tertiary creep
950° C/400MPa

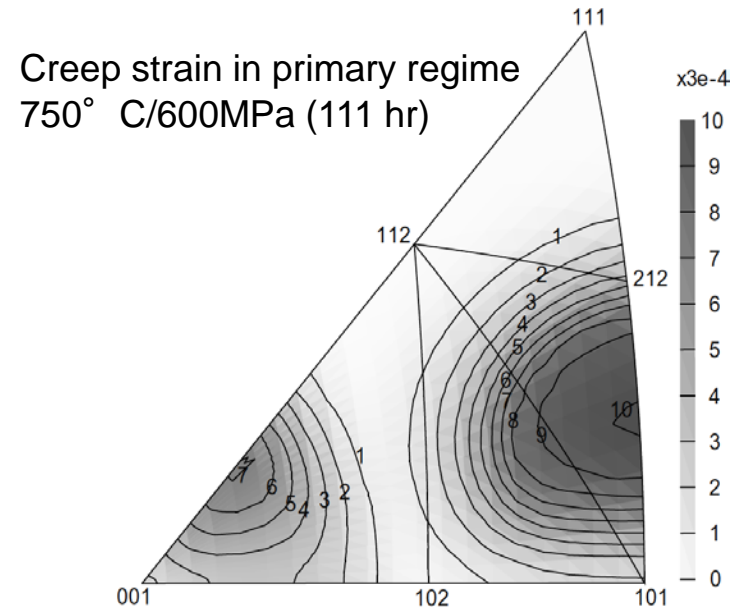
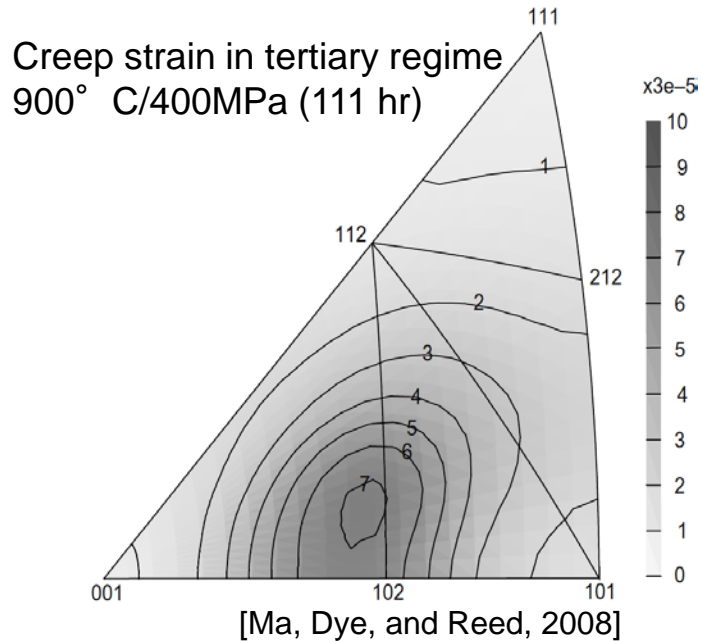


Primary creep
750° C/770MPa



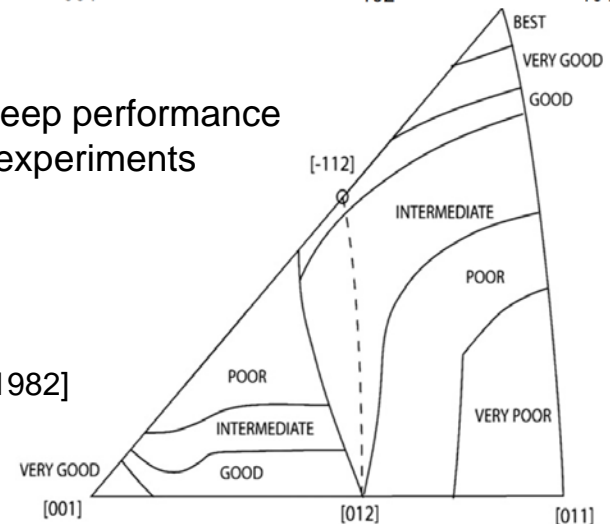
Deformation along [001]
Volume fraction of C' fixed at 0.7

CMSX-4 Model Predictions

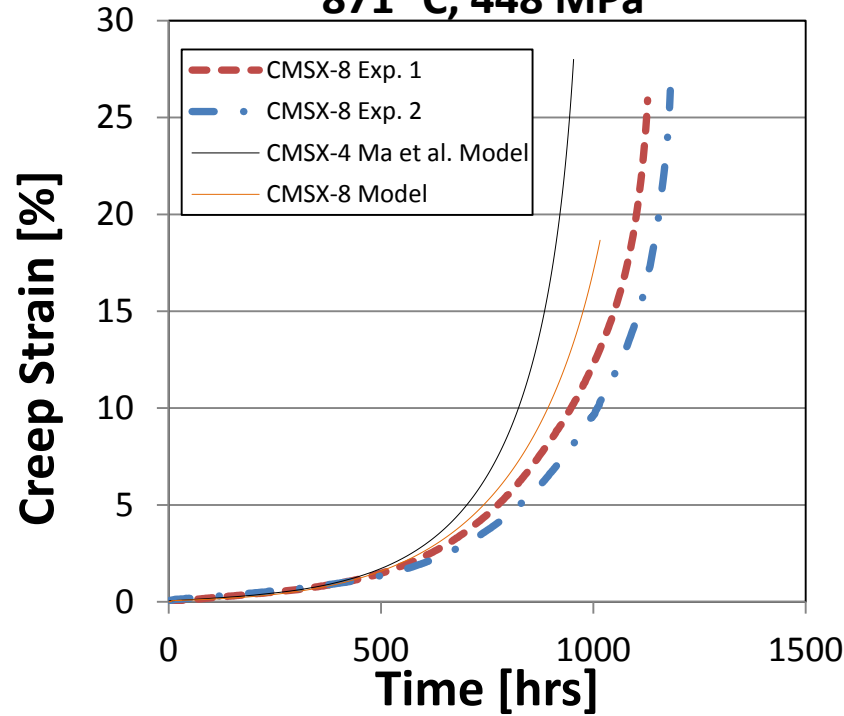


Primary creep performance based on experiments

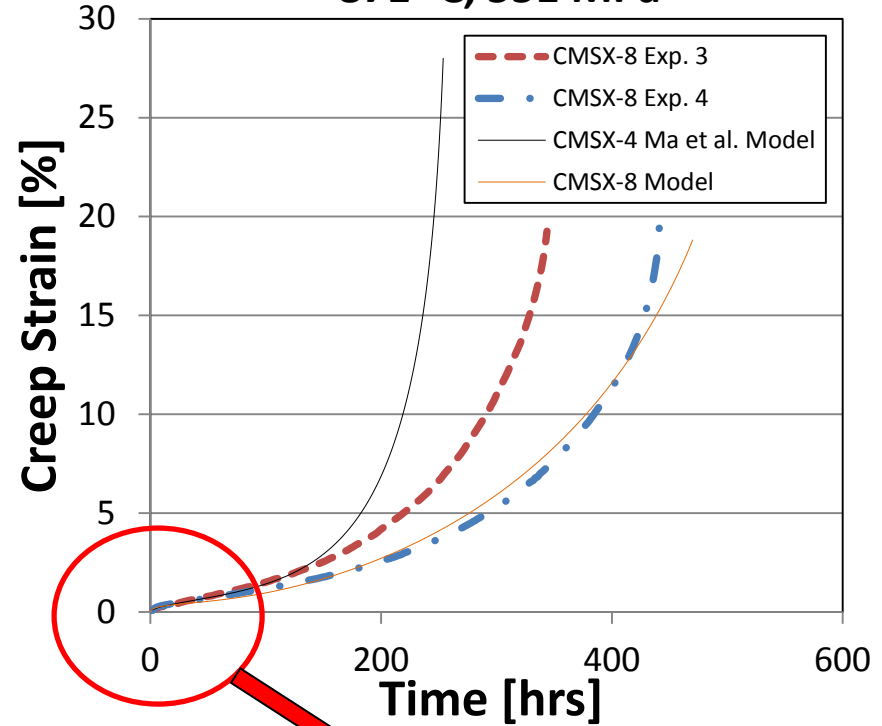
[MacKay and Meier, 1982]



871 °C, 448 MPa

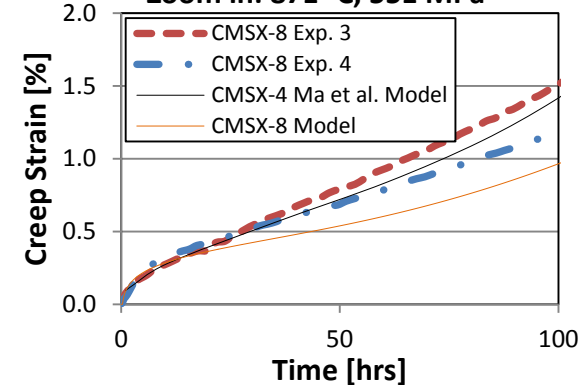


871 °C, 551 MPa



Primary, secondary and tertiary creep can be captured with the model

Zoom in: 871 °C, 551 MPa



- Directional coarsening is roughly a constant volume process
- Stress-free coarsening maintains proportionality between all precipitate/channel dimensions
- Microstructure uniqueness is defined by 2 independent dimensions

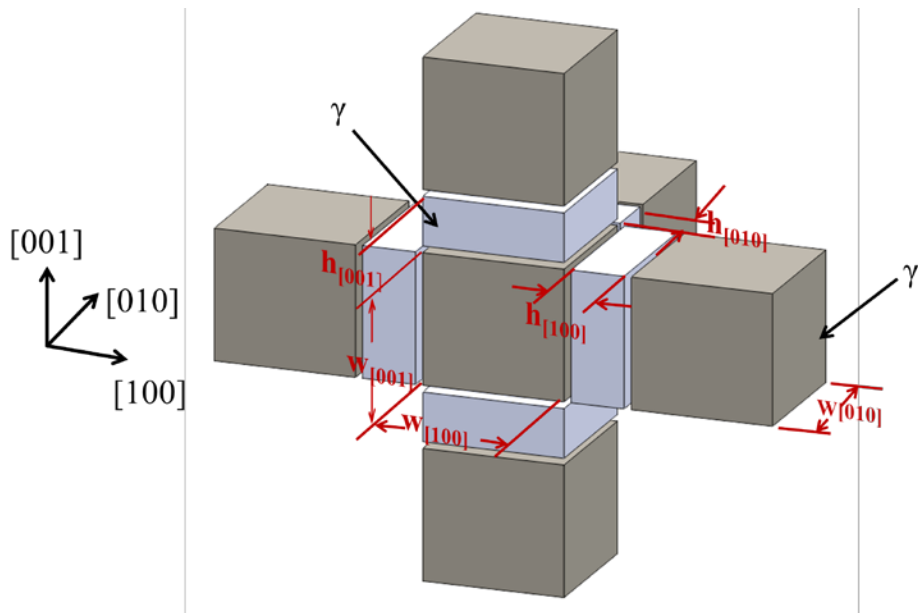
Rafting:
$$\dot{w}_i^{raft}(T, \sigma) = - \left(\frac{3Aw_i}{2w_o} \right) \left(\frac{\sigma_i^{dev}}{\sigma_{VM} + \delta} \right) \exp \left(- \frac{Q_{raft} - \sigma_{VM}U(T)}{RT} \right)$$
 [Tinga, Brekelmans, and Geers, 2009]

Isotropic Coarsening:
$$\dot{w}_i^{coar} = \frac{8K}{3} (w_o^3 + 8Kt)^{-\frac{2}{3}}$$

$$\dot{w}_i = \dot{w}_i^{coar} + \dot{w}_i^{raft}$$

$$\eta = \frac{h_{[001]} - h_{[001]}^o}{h_{[001]}^o}$$

$$\zeta = \frac{h_{[100]} - h_{[100]}^o}{h_{[100]}^o}$$



Since Re segregates almost exclusively in the γ channels, the Activation energy in the γ phase can be modified to account for Re content as follows:

$$\left\{ \begin{array}{l} \dot{\gamma}_{\gamma}^{in(\alpha)} = \Theta(T) \rho_{\gamma}^{(\alpha)} b \lambda_{\gamma}^{(\alpha)} F_{attack} \text{sign}(\tau^{(\alpha)} + \tau_{mis}^{(\alpha)} - \chi^{(\alpha)}) \exp \left\{ \frac{-Q_{slip}^{110} + \left(\left| \tau^{(\alpha)} + \tau_{mis}^{(\alpha)} - \chi^{(\alpha)} \right| - \tau_{\gamma pass}^{(\alpha)} - \tau_{oro}^{(\alpha)} \right) V_{c1}^{(\alpha)}}{kT} \right\} \\ \dot{\gamma}_{Ll_2}^{in(\alpha)} = \rho_{Ll_2}^{(\alpha)} b \lambda_{Ll_2}^{(\alpha)} F_{attack} \text{sign}(\tau^{(\alpha)} - \chi^{(\alpha)}) \exp \left\{ \frac{-Q_{slip}^{112} + \left(\left| \tau^{(\alpha)} - \chi^{(\alpha)} \right| - \tau_{Ll_2 pass}^{(\alpha)} - \tau_{APB} \right) V_{c2}^{(\alpha)}}{kT} \right\} \end{array} \right.$$

If we considering activation energy for plastic flow Q_o a function of %Re, the diffusivity parameter could take the form of:

$$\Theta(T) = \exp\left(-\frac{Q_o}{RT}\right) \quad \text{for } T \geq \frac{T_m}{2} \qquad \Theta(T) = \exp\left(-\frac{2Q_o}{RT} \left[\ln\left(\frac{T_m}{2T}\right) + 1 \right]\right) \quad \text{for } T \leq \frac{T_m}{2}$$